

Neutrino mean free path for proto–neutron star matter within the Skyrme model

E. Bauer^{1,2}, J. Torres Patiño¹, and O. G. Benvenuto^{2,3}

¹*Instituto de Física La Plata, IFLP, CCT-CONICET-UNLP, La Plata 1900, Argentina*

²*Facultad de Ciencias Astronómicas y Geofísicas, Universidad Nacional de La Plata, La Plata 1900, Argentina*

³*Instituto de Astrofísica de La Plata, IALP, CCT-CONICET-UNLP, La Plata 1900, Argentina*



(Received 23 November 2022; revised 7 May 2023; accepted 30 May 2023; published 12 June 2023)

The neutrino mean free path is evaluated in hot proto–neutron star matter under a strong magnetic field. We consider densities in the range $0.04 \leq \rho \leq 0.4 \text{ fm}^{-3}$, several proton fractions from symmetric matter up to pure neutron matter, temperatures up to 30 MeV, and two magnetic field strengths $B = 10^{17}$ and 10^{18} G. Polarized proto–neutron star matter is described within the nonrelativistic Hartree-Fock model using the LNS Skyrme interaction, where the proper treatment for instabilities for low densities and temperatures is implemented. Under the same conditions, the degree of polarization of protons is stronger than the one for neutrons. For the neutrino mean free path we consider three reactions: the neutrino-neutron and neutrino-proton scattering, $\nu + n \rightarrow \nu' + n'$ and $\nu + p \rightarrow \nu' + p'$, respectively, and the neutrino absorption reaction $\nu + n \rightarrow e^- + p$. The magnetic field induces an asymmetry in the mean free path which favors the flux of neutrinos parallel to the magnetic field in the case of neutron scattering and the absorption reaction, whereas it is antiparallel in the case of proton scattering. For most of the conditions the absorption reaction is the dominant one. The dependence of the neutrino mean free path on the magnetic field, the temperature, and the proton fraction is different for each reaction. As a representative case of our results, the asymmetry in the mean free path is $\approx 21\%$ at saturation density for $B = 10^{18}$ G, $T = 15$ MeV, and symmetric matter, while we have $\approx -1\%$ for $B = 10^{17}$ G and the same values of all the other conditions.

DOI: [10.1103/PhysRevC.107.065804](https://doi.org/10.1103/PhysRevC.107.065804)

I. INTRODUCTION

The neutrino physics is important to understand many astrophysical problems. In particular, they play a fundamental role all over the stages of the collapse of a massive star, starting from the supernova explosions [1–11], the early development of compact stellar remnants [12–14], to the neutron star cooling [15,16] and merging of neutron stars [17–21]. There are many mechanisms which produce neutrinos. Just to name a few of them, we have direct Urca, modified Urca, baryon bremsstrahlung, and Coulomb bremsstrahlung, which are mainly originated from the neutron star core, while processes like electron-positron annihilation, plasmon decay, and electron-nucleus bremsstrahlung are attributed to the neutron star crust (a discussion of these different mechanisms can be found in Refs. [22,23]). The transport properties of neutrinos are necessary for a good understanding of stellar evolution. These properties are modified by the presence of strong magnetic fields. In the case of the so-called magnetars, the magnetic field intensity can reach values up to 10^{14} – 10^{15} G at the star surface and it can grow by several orders of magnitude in its dense interior [24]. In fact, the emission of neutrinos is expected to depend on the direction of the magnetic field. This asymmetrical emission of neutrinos has been suggested as a possible mechanism to explain the “pulsar kick problem”: the observation that pulsars do not move with the velocity of their progenitor star, but rather with a substantially greater speed [25].

Several mechanisms have been suggested as possible explanations for the pulsar kick problem. Some of them do not involve neutrinos, like an asymmetry in the gravitational collapse of the progenitor, acceleration due to the pulsar electromagnetic radiation, or the evolution of a binary system which may produce rapidly moving pulsars. Another possible mechanism is the asymmetrical emission of neutrinos, because an asymmetry as small as $\approx 1\%$ would be enough to explain the pulsar movement. The asymmetrical emission of neutrinos can have two different origins. Neutrino oscillation can be altered by the magnetic field, resulting in an anisotropy in the momentum of the outgoing neutrinos [26]. A second source is the neutrino parity violation, which can also induce an asymmetry on the emission when multiple scattering of neutrinos in polarized matter is taken into account [27–30]. This last possibility is the one which we explore in this work. In particular, we evaluate the neutrino mean free path (NMFP), for hot polarized proto–neutron star matter.

The NMFP in dense matter has been studied with and without the presence of a magnetic field by many authors using various approximation schemes. It has been extensively discussed in the absence of magnetic field (see, e.g., Refs. [31–44] and references therein). There are also many works which discussed the NMFP in the presence of a strong magnetic field (see, e.g., Refs. [26,27,45–54]). To model the NMFP, an equation of state (EOS) is required to describe the medium in which the neutrino is moving. In addition, we need

a scheme to describe the interaction of the neutrino with the particles of this dense medium. Note that the neutrino cross section is evaluated both in free space and in a dense medium. The weak transition matrix element for both cases is basically the same. The cross section in a dense medium incorporates particle distribution functions which limits the phase space of the particles involved in the neutrino reactions. These particle distribution functions use the single-particle energies and chemical potential from the EOS. The magnetic field induces a quantization for the charge particles in the medium, called the Landau quantization. Obviously this quantization affects both the EOS and the wave functions of initial and final particles required in the weak transition matrix element, as long as they are charged particles.

In this work we study the NMFP in hot proto-neutron star matter with a strong magnetic field and a fixed proton fraction. In previous works we analyzed pure neutron matter, considering the inelastic neutrino-neutron scattering and the absorption of a neutrino by a neutron [53,54]. A set of the possible reactions of a neutrino can be found in Ref. [39]. The evaluation of the NMFP starts with the EOS. For hot polarized proto-neutron star matter, the EOS is developed within the nonrelativistic Hartree-Fock model using the LNS Skyrme interaction [55]. With a different nuclear interaction, this EOS was already developed in Ref. [56]. For systems with two or more different kinds of particles, the nuclear interaction induces an instability for low temperatures and densities. The stability is restored by splitting the system into two phases, with different densities, spin, and isospin composition for each phase. Once the EOS is established, one has to choose a set of reactions between the neutrino and the particles present in the medium. In our case, we consider the neutrino-proton and -neutron scattering reactions, together with the absorption one. The evaluation of the NMFP for each reaction shows that their functional behavior with density, temperature, magnetic field, and proton fraction is different. We consider that these variables are locally constants, due to the scale of the reaction. Then we evaluate the asymmetry in the NMFP.

The work is organized as follows. In Sec. II, we develop the formalism for the calculation of the NMFP. This is done in four parts: in Sec. II A, we outline the EOS for hot polarized proto-neutron star matter; in Sec. II B, we give some details on the instability region; in Sec. II C, we discuss the initial wave function for our problem; and in Sec. II D, we give an analytical expression for the neutrino-proton scattering. Note that the corresponding expressions for the neutrino-neutron and absorption cross section are already given in Refs. [53] and [54], respectively. In Sec. III, we discuss our results, putting special emphasis on the asymmetry in the NMFP. Finally, in Sec. IV, we give the conclusions of our work.

II. THE NEUTRINO MEAN FREE PATH

In this section we present expressions for the NMFP (λ), for hot nonrelativistic proto-neutron star matter under a strong constant magnetic field and for a fixed value for the proton fraction. The model for the EOS of matter fulfilling these conditions is discussed in the next section.

To evaluate the NMFP, we consider the following reactions: first, the scattering reactions,

$$\nu_i + n_i \rightarrow \nu_f + n_f, \quad (1)$$

$$\nu_i + p_i \rightarrow \nu_f + p_f, \quad (2)$$

and second, the absorption reaction,

$$\nu_i + n_i \rightarrow e_f^- + p_f. \quad (3)$$

Reactions (1) and (3) were studied for pure neutron matter in Refs. [53] and [54], respectively. For proto-neutron star matter the results for these reactions change, as for a fixed baryonic density, the neutron density is smaller. This point is discussed in detail in Sec. III. Explicit expressions for reaction (2) are given in this section.

A. Polarized proto-neutron star matter in the Skyrme model

For the benefit of the reader, in this section we resume the model developed in Ref. [56], with the addition of some details needed for the NMFP. To obtain the EOS we employ the Hartree-Fock approximation with the Skyrme effective nuclear interaction. This scheme allows us to find an energy density functional, which is a convenient way to study thermodynamic properties of the system. For simplicity, this is named the Skyrme model. Details on the particular parametrization of the Skyrme interaction are left to Sec. III.

The inputs of our EOS model are the baryonic density, the proton fraction, the temperature, and the magnetic field. In a neutron star there is a spatial dependence on these quantities. In particular, we consider a constant magnetic field in the \hat{z} direction, $\vec{B} = B\hat{k}$. For the whole neutron star one can implement a realistic model for the magnetic field, as well as for the density and the temperature. The curvature of the magnetic field from a realistic model would allow us to consider it as locally uniform due to the scale of the reactions under consideration. Analogous hypotheses are valid for both density and temperature. From the EOS we obtain the single-particle energies of protons and neutrons, their chemical potentials, and spin asymmetries. These magnitudes are needed for the evaluation of the NMFP.

The magnetic field modifies the single-particle spectra of the standard Skyrme model. In the first place, there is a direct coupling between nucleons and the magnetic field, due to their intrinsic magnetic moments leading to an additional term $-\mu_N B s_{p,n} g_{p,n}$, where μ_N is the Bohr magneton ($\mu_N \cong 3.15245 \times 10^{-18}$ MeV/G), $s_{p,n}$ is the spin z projection and the g factors take account of the anomalous magnetic moments with values $g_p = 2.793$ and $g_n = -1.913$, for protons and neutrons, respectively. Furthermore, for protons the magnetic field induces a quantization of the energy spectra. In the case of a uniform field, the dynamics of the problem exhibits quantized eigenvalues associated with the motion in the plane orthogonal to the applied field. They are oscillatorlike levels, depending on a discrete quantum number in the form $(N_p + 1/2) \omega_p$, with $\omega_p = eB/m_p$ being the cyclotron frequency for each particle. This is known as Landau quantization and the quantum number N_p takes the same values as the quantum oscillator. We show now the single-particle energies for the

protons and neutrons,

$$E_{s_p}(p_z, N_p) = m_p + \frac{p_z^2}{2m_{s_p}^*} + \frac{1}{8}v_{s_p} + \mu_p B(2N_p + 1 - s_p g_p), \quad (4)$$

$$E_{s_n}(\vec{p}) = m_n + \frac{p^2}{2m_{s_n}^*} + \frac{1}{8}v_{s_n} - \mu_n B s_n g_n, \quad (5)$$

where \vec{p} is the momentum and p_z its z projection. Note that s_j takes the values $+1$ (-1) for spin up (down). The nuclear effective interaction is present through the effective nucleon masses $m_{s_p(n)}^*$ and the single-particle Skyrme potential energy $v_{s_p(n)}$, having the explicit expressions

$$\frac{1}{m_{s_i}^*} = \frac{1}{m_i} + \frac{1}{4}\rho(b_0 - b_2 w I_i) + \frac{1}{4}s_i \sum_j (b_1 + I_i I_j b_3) W_j \quad (6)$$

and

$$v_{s_i} = (a_0 - a_2 w I_i)\rho + \sum_{j, s'_j} (b_0 + I_i I_j b_2) K_{j, s'_j} + s_i \sum_j (a_1 + a_3 I_i I_j) W_j + s_i \sum_{j, s'_j} s'_j (b_1 + b_3 I_i I_j) K_{j, s'_j}, \quad (7)$$

with $i, j = p, n$ and we have defined $I_p = 1$ and $I_n = -1$. The isospin asymmetry fraction is $w = (\rho_n - \rho_p)/\rho$, where $\rho = \rho_n + \rho_p$. Since the spin states are not symmetrically occupied, one can define for each isotopic component the number density of particles with a given spin polarization ρ_{i, s_i} . The spin asymmetry density W_i gives a measure of the spin polarization $W_i = \sum_{s_i} s_i \rho_{i, s_i}$. The expressions for the kinetic energy density K_{i, s_i} are presented below. The coefficients a_l and b_l are built up from the Skyrme interaction according to

$$\begin{aligned} a_0 &= 6t_0 + t_3 \rho^\sigma, \\ b_0 &= [3t_1 + t_2(5 + 4x_2)]/2, \\ a_1 &= -2t_0(1 - 2x_0) - t_3(1 - 2x_3)\rho^\sigma/3, \\ b_1 &= [t_2(1 + 2x_2) - t_1(1 - 2x_1)]/2, \\ a_2 &= -2t_0(1 + 2x_0) - t_3(1 + 2x_3)\rho^\sigma/3, \\ b_2 &= [t_2(1 + 2x_2) - t_1(1 + 2x_1)]/2, \\ a_3 &= -2t_0 - t_3 \rho^\sigma/3, \\ b_3 &= (t_2 - t_1)/2, \end{aligned}$$

where the different constants appearing on the right-hand side (rhs) of these expressions are standard coefficients for the Skyrme interaction (see, for instance, Ref. [55]).

We show now the expressions for the spin number densities ρ_{i, s_i} , the spin asymmetry density W_i , and the kinetic energy density K_{i, s_i} , for each particle:

$$\rho_{p, s_p} = \frac{eB}{(2\pi)^2} \sum_{N_p=0}^{\infty} \int_{-\infty}^{\infty} dp_z f(E_{s_p}, \mu_p, T), \quad (8)$$

$$W_p = \frac{eB}{(2\pi)^2} \sum_{s_p, N_p} s_p \int_{-\infty}^{\infty} dp_z f(E_{s_p}, \mu_p, T), \quad (9)$$

$$K_{p, s_p} = \frac{eB}{(2\pi)^2} \sum_{N_p} \int_{-\infty}^{\infty} dp_z p_z^2 f(E_{s_p}, \mu_p, T), \quad (10)$$

$$\rho_{n, s_n} = \frac{1}{(2\pi)^3} \int d^3 p f(E_{s_n}, \mu_n, T), \quad (11)$$

$$W_n = \sum_{s_n} \frac{s_n}{(2\pi)^3} \int d^3 p f(E_{s_n}, \mu_n, T), \quad (12)$$

$$K_{n, s_n} = \frac{1}{(2\pi)^3} \int d^3 p p^2 f(E_{s_n}, \mu_n, T). \quad (13)$$

Here $\mu_{p(n)}$ is the chemical potential. The parameter T stands for the temperature. In thermal equilibrium $f(E_{s_i}, \mu_i, T)$ is given by the Fermi-Dirac particle distribution function,

$$f(E_{s_i}, \mu_i, T) = \frac{1}{1 + \exp[(E_{s_i} - \mu_i)/T]}. \quad (14)$$

Owing to the minimization of the thermodynamic potential, the chemical potential cannot depend on the spin projection. But the single-particle energy E_{s_j} does, which allows the possibility that $\rho_{i, s_i=+1} \neq \rho_{i, s_i=-1}$. Instead of working with W_i , it is convenient to define a dimensionless spin asymmetry A_i ,

$$A_i \equiv \frac{\rho_{i, s_i=+1} - \rho_{i, s_i=-1}}{\rho_{i, s_i=+1} + \rho_{i, s_i=-1}} = \frac{W_i}{\rho_i}, \quad (15)$$

where $\rho_i = \rho_{i, s_i=+1} + \rho_{i, s_i=-1}$. Note that we have two independent spin asymmetries: A_n and A_p .

Now we have all the elements to show the thermodynamic potential. The energy density is given by

$$\begin{aligned} \mathcal{E} &= \sum_{i, s_i} \frac{K_{i, s_i}}{2m_{i, s_i}^*} + \frac{1}{16} \left[a_1 \left(\sum_i W_i \right)^2 + a_3 \left(\sum_i I_i W_i \right)^2 \right. \\ &\quad \left. + (a_0 + a_2 w^2) \rho^2 \right] + \mu_n B(2L + \rho_p - g_p W_p - g_n W_n), \end{aligned} \quad (16)$$

where $\rho = \rho_p + \rho_n$ and

$$L = \frac{eB}{(2\pi)^2} \sum_{s_p, N_p} N_p \int_{-\infty}^{\infty} dp_z f(E_{s_p}, \mu_p, T). \quad (17)$$

For completeness we also show the expression for the entropy density \mathcal{S} ,

$$\begin{aligned} \mathcal{S} &= \mathcal{S}_p + \mathcal{S}_n, \\ \mathcal{S}_p &= -\frac{eB}{(2\pi)^2} \sum_{s_p, N_p} \int_{-\infty}^{\infty} dp_z \{ f(E_{s_p}, \mu_p, T) \ln [f(E_{s_p}, \mu_p, T)] \\ &\quad + [1 - f(E_{s_p}, \mu_p, T)] \ln [1 - f(E_{s_p}, \mu_p, T)] \}, \\ \mathcal{S}_n &= \sum_{s_n} \frac{1}{(2\pi)^3} \int d^3 p \{ f(E_{s_n}, \mu_n, T) \ln [f(E_{s_n}, \mu_n, T)] \\ &\quad + [1 - f(E_{s_n}, \mu_n, T)] \ln [1 - f(E_{s_n}, \mu_n, T)] \}. \end{aligned}$$

The entropy is needed to build up the free energy $\mathcal{F} = \mathcal{E} - T\mathcal{S}$ and the pressure $P = \sum_a \mu_a n_a - \mathcal{F}$.

We can ascribe the free energy the following functional dependence,

$$\mathcal{F} = \mathcal{F}(\rho_{s_p=1}, \rho_{s_p=-1}, \rho_{s_n=1}, \rho_{s_n=-1}, T, B), \quad (18)$$

with two constraints:

$$\rho = \rho_{s_p=1} + \rho_{s_p=-1} + \rho_{s_n=1} + \rho_{s_n=-1}, \quad (19)$$

$$w = \frac{1}{\rho} (\rho_n - \rho_p). \quad (20)$$

The inputs of our problem are ρ , w , B , and T . Then the partial densities ρ_{i, s_i} are varied to find the minimum of the free energy \mathcal{F} , which represents the physical state. The knowledge of these partial densities implies the knowledge of the single-particle energies, chemical potential, and spin asymmetries. From this analysis it is clear that the system is polarized by the action of the magnetic field. The degree of polarization is given by the spin asymmetry. In general, the system is partially polarized: there is a competition among the Pauli principle which favors an equal number of nucleons with spin up and down, and the magnetic field, which tries to align all spin projections in the same direction. The minimum of \mathcal{F} is usually a partial polarization. As we show soon in this section, these quantities are required in the evaluation of the NMFP.

B. Coexistence of phases in proto-neutron star matter

For certain conditions of low densities and temperatures, the nuclear interaction favors a phase transition into a nonuniform system [57–60]. For proto-neutron star matter, the system splits into two coexisting phases, one of low density and the other one with higher density, which are interpreted as a gas-liquid system. Moreover, for nonsymmetric matter the isospin composition of each phase is different. This is a general property of all thermodynamic systems with two or more different kinds of particles, with or without magnetic field. Now we focus on our particular system. Starting at low densities for fixed values for the temperature, magnetic field, and proton fraction, the system shows a small amount of the liquid phase which grows until the gas disappears and the system is uniform again. The EOS described in the previous section predicts this phase transition by showing an instability. To be clear, this instability is sometimes depicted in the EOS by decreasing values of the pressure when the density increases, even taking negative values. There are also more subtle behaviors such as a change in the curvature of the pressure. We refer the reader to the work of Chomaz *et al.* [59] for a complete discussion on the subject. In this section we show some simple elements needed in the evaluation of the NMFP.

Let us denote with the superscripts a and b the gas and liquid phases, respectively. The system is stable against separation into two phases when

$$\mathcal{F}(\rho, T, B) < (1 - \alpha) \mathcal{F}(\rho^a, T, B) + \alpha \mathcal{F}(\rho^b, T, B), \quad (21)$$

for any value of α in the range $0 \leq \alpha \leq 1$. In this expression we simplified the density dependence for convenience. The actual dependence is the one in Eq. (18). The instability is

the density region where condition (21) is not fulfilled. The new equilibrium is reached when the following conditions are satisfied,

$$\begin{aligned} P(\rho_{s_p=1}^a, \rho_{s_p=-1}^a, \rho_{s_n=1}^a, \rho_{s_n=-1}^a, T, B) \\ = P(\rho_{s_p=1}^b, \rho_{s_p=-1}^b, \rho_{s_n=1}^b, \rho_{s_n=-1}^b, T, B), \end{aligned} \quad (22)$$

$$\begin{aligned} \mu_p(\rho_{s_p=1}^a, \rho_{s_p=-1}^a, \rho_{s_n=1}^a, \rho_{s_n=-1}^a, T, B) \\ = \mu_p(\rho_{s_p=1}^b, \rho_{s_p=-1}^b, \rho_{s_n=1}^b, \rho_{s_n=-1}^b, T, B), \end{aligned} \quad (23)$$

$$\begin{aligned} \mu_n(\rho_{s_p=1}^a, \rho_{s_p=-1}^a, \rho_{s_n=1}^a, \rho_{s_n=-1}^a, T, B) \\ = \mu_n(\rho_{s_p=1}^b, \rho_{s_p=-1}^b, \rho_{s_n=1}^b, \rho_{s_n=-1}^b, T, B), \end{aligned} \quad (24)$$

with the constraints

$$\rho = (1 - \alpha) \rho^a + \alpha \rho^b, \quad (25)$$

$$\omega \rho = (1 - \alpha) \omega^a \rho^a + \alpha \omega^b \rho^b, \quad (26)$$

where $\rho^{a(b)} = \rho_n^{a(b)} + \rho_p^{a(b)}$ and $\omega^{a(b)} = (\rho_n^{a(b)} - \rho_p^{a(b)}) / (\rho_n^{a(b)} + \rho_p^{a(b)})$. Equations (25) and (26) tell us that the total baryonic density and isospin asymmetry are conserved. The solution of these sets of equations is quite involved and their results are known as Gibbs construction (for technical details see Ref. [59] and references therein). By hypothesis, the instability region starts with a uniform system with density ρ^a and ends with also a uniform system with density ρ^b . But from the beginning of the instability region these partial densities change. Not only the values of ρ^a and ρ^b , but also their spin and isospin composition vary along the instability region, constrained by conditions (25) and (26). In our case, the ω value is fixed and the partial densities $\rho_{s_i}^{a(b)}$, together with the parameter α , are evaluated for each value of ρ within the instability region.

From the Gibbs construction, the value of the pressure within the instability region is obtained. An important quantity for our problem is the spin asymmetry density, W_i ($i = p, n$). It is easily calculated as

$$W_i = (1 - \alpha) W_i^a + \alpha W_i^b. \quad (27)$$

Within the instability region this value differs from the one of a uniform system. For further use, it is convenient to show also the spin asymmetry fraction, A_i :

$$A_i = \frac{1}{\rho_i} [(1 - \alpha) A_i^a \rho_i^a + \alpha A_i^b \rho_i^b]. \quad (28)$$

Having all these elements, to evaluate the NMFP first we calculate the partial values λ^a and λ^b (the NMFPs for the systems “ a ” and “ b ,” respectively). Then we have

$$\frac{1}{\lambda} = \frac{1 - \alpha}{\lambda^a} + \frac{\alpha}{\lambda^b}. \quad (29)$$

The total baryonic density for this λ is implicitly contained in the values of ρ^a , ρ^b , and α . Our concern is the asymmetry in the NMFP due to the presence of a strong magnetic field. Beyond its actual relevance, a reliable evaluation of this asymmetry requires the construction in Eq. (29).

The Gibbs construction is required for asymmetric matter. Neutron matter ($w = 1$) shows no instability, whereas symmetric matter ($w = 0$) is much simpler as it requires the

Maxwell construction [58]. Briefly, when the pressure is plotted against the volume it shows a local minimum followed by a local maximum. The Maxwell construction of equal areas gives us ρ^a and ρ^b , the values for the total baryonic density at both ends of the instability region, which remain unchanged along the instability region. In this case only the parameter α varies. It does so monotonously according to Eq. (25): $\alpha = (\rho - \rho^a)/(\rho^b - \rho^a)$. Also λ^a and λ^b are fixed by the values at both extremes of the instability region. Therefore, the evaluation of λ for different densities is straightforward from Eq. (29).

A further point which deserves attention is that, for low temperatures and subnuclear densities, there may exist non-homogeneous matter in different geometric structures, called a pasta phase, which result from the competition between the Coulomb and the strong interaction [61]. Most of these models are developed at zero temperature. The effect of the magnetic field over the pasta phase was studied recently (see Ref. [62] and references therein). In these works it is discussed that strong magnetic fields cause an extension of the inner crust of the neutron stars and an increase of the proton fraction, among other effects. However, the effect of the magnetic field is washed out for temperatures bigger than 10^9 K (≈ 0.09 MeV) [63]. The pasta phase represents another kind of nonhomogeneous possible state of matter. However, the study of the NMFP in the pasta phase goes beyond the scope of this work.

C. Initial spin wave function for protons and neutrons

To evaluate the NMFP we employ Fermi's golden rule, where we sum up over all possible final states and average over the initial states, as long as we do not know which is the initial state. In this section we show that the knowledge of the spin polarization from the EOS gives us the information over the initial spin wave function. This section is also a summary of the more complete discussion in Ref. [53].

The polarization of the system is an average property, which can be parametrized by means of the spin asymmetries A_p and A_n . These asymmetries depend on the baryonic density, the temperature, and the intensity of the magnetic field. The chemical potential of protons and neutrons also depends on the magnetic field. To learn more about the polarization, we consider a small volume V inside the neutron star, for which the density, temperature, and magnetic field can be considered as constant. To study the spin polarization of a set of N_i particles ($i = p, n$) within this volume, we have to evaluate

$$\langle \hat{S}_{i,z} \rangle_{\text{System}} = \left(\frac{N_{i,s_z=+1} - N_{i,s_z=-1}}{N_{i,s_z=+1} + N_{i,s_z=-1}} \right) \frac{\hbar}{2}, \quad (30)$$

where $\hat{S}_{i,z}$ is the spin projection operator in the z axis for the particle i ; $N_{i,s_z=+1}$ and $N_{i,s_z=-1}$ are the numbers of i particles with spin up and down, respectively. Note that $N_i = N_{i,s_z=+1} + N_{i,s_z=-1}$. Writing now $N_{i,s_z=\pm 1} = V \rho_{i,s_z=\pm 1}$ and using the definition of the spin asymmetry A_i in Eq. (15), it

is easy to see that

$$\langle \hat{S}_{i,z} \rangle_{\text{System}} = A_i \frac{\hbar}{2}. \quad (31)$$

Now we have to establish a link between A_i , which is a global property of the particles within V , and the wave function of a single particle. This is simple, because we know that the mean value of the operator $\hat{S}_{i,z}$ evaluated with the wave function of particle i must have the same value as the one from the whole system [64]. More explicitly, if particle i has a spinor $|U_i\rangle$, we have

$$\langle U_i | \hat{S}_{i,z} | U_i \rangle = \langle \hat{S}_{i,z} \rangle_{\text{System}}. \quad (32)$$

The left-hand side (lhs) in this equality is a matrix element of a single particle, while the rhs is an average from all particles within V . After some algebra, we get (for more details see Appendix B in Ref. [53])

$$|U_i\rangle = \sqrt{\frac{1+A_i}{2}} |U_{i,s_i=+1}\rangle + \sqrt{\frac{1-A_i}{2}} |U_{i,s_i=-1}\rangle, \quad (33)$$

with $i = p, n$.

In this expression the ket $|U_{i,s_i=+1}\rangle$ ($|U_{i,s_i=-1}\rangle$) is the spin-up (spin-down) spinor for the i particle. As we know the initial spin component of the wave function, it is not necessary to average over the initial spin state.

D. The neutrino-proton scattering cross section for a polarized system

In this section we show an expression for the inelastic neutrino-proton scattering cross section per unit volume for a polarized system. The NMFP is the inverse of this cross section. The cross section for the reaction $\nu_i + p_i \rightarrow \nu_f + p_f$ can be written as

$$\frac{\sigma_{\text{protscatt}}(\vec{p}_{\nu_i})}{V} = \int d\Pi_{\nu_f} \int d\Pi_{p_f} \int d\Pi_{p_i} \mathcal{W}_{fi}^{\text{prot}} \times [1 - f(E_{s_{p_f}}, \mu_p, T)] f(E_{s_{p_i}}, \mu_p, T), \quad (34)$$

where the symbol $\int d\Pi_j$ represents the summation over all possible states of particle j and it is defined soon.

We focus on the transition rate $\mathcal{W}_{fi}^{\text{prot}}$. The indices i and f stand for the initial and final states, respectively. To evaluate the transition rate we employ the scattering operator \hat{S} , given by $\hat{S} = \hat{U}(-\infty, \infty)$, where $\hat{U}(t_2, t_1)$ is the time-evolution operator [65]. By keeping only the leading term, we have

$$\hat{S} = i \int d^4x \hat{\mathcal{H}}_{\text{int}}, \quad (35)$$

where $\hat{\mathcal{H}}_{\text{int}}$ is the Hamiltonian density. We employ an effective Hamiltonian which is the low-momentum limit of the weak vertex from the standard model (see, for instance,

Ref. [38]),

$$\hat{\mathcal{H}}_{\text{int}} = \frac{G_F}{\sqrt{2}} \bar{\Psi}_{p_f} \gamma_\mu (C_V - C_A \gamma_5) \Psi_{p_i} \bar{\Psi}_{\nu_f} \gamma^\mu (1 - \gamma_5) \Psi_{\nu_i} + \text{H.c.} \quad (36)$$

In this expression Ψ_j is the field operator for particle j . Here G_F is the Fermi weak-coupling constant ($G_F/(\hbar c)^3 = 1.16637(1) \times 10^{-5} \text{ GeV}^{-2}$). For the vector and axial-vector couplings we have $C_V = 0.08$ and $C_A = 1.23$, respectively. These values are taken from Ref. [38].

The scattering matrix S_{fi} is the \hat{S} operator evaluated between the initial and final states. The square of S_{fi} , divided by time, is the transition rate:

$$\mathcal{W}_{fi}^{\text{prot}} = \frac{|S_{fi}|^2}{\mathcal{T}}, \quad (37)$$

where \mathcal{T} is the time interval where the transition takes place [66].

A complete discussion of the wave functions for all particles is given in Appendix A in Ref. [54]. For the benefit of the reader, it is convenient to reproduce here the proton wave function, where the spatial dependence is expressed in

cylindrical coordinates (ρ, ϕ, z) ,

$$\psi_p(\rho, \phi, z, t) = L^{-1/2} e^{i(p_{p,z}z - E_p t)} \left(\frac{eB}{2\pi} \right)^{1/2} \times e^{i(R_p - N_p)\phi} I_{R_p, N_p}(\xi) U_p, \quad (38)$$

where U_p is the proton spinor which was discussed in Sec. II C. The index N_p is the energy level quantum number for the proton Landau state. The explicit expression for the function $I_{R_p, N_p}(\xi)$ is given by

$$I_{R_p, N_p}(\xi) = \left(\frac{N_p!}{R_p!} \right)^{1/2} e^{-\xi/2} \xi^{(R_p - N_p)/2} \mathcal{L}_{N_p}^{R_p - N_p}(\xi), \quad (39)$$

with $\xi = eB \rho^2/2$ and for the definition of the Laguerre polynomials \mathcal{L}_j^i we adopted the one from Ref. [67]. The R_p is called the radial quantum number and its values are discussed in Appendix A in Ref. [54], together with the neutrino wave function. All wave functions are normalized in a volume $V = \mathcal{L}\mathcal{A}$, where L is the length along the z axis and \mathcal{A} is the area in the perpendicular plane.

Using these wave functions together with the interaction in Eq. (36), and after some algebra, the S_{fi} matrix for the proton is given by

$$S_{fi}^{\text{prot}} = i \frac{G_F}{\sqrt{2}} L^{-1} V^{-1} (2\pi)^2 \delta(E_{p_f} + |p_{v_f}| - E_{p_i} - |p_{v_i}|) \delta(p_{p_f,z} + p_{v_f,z} - p_{p_i,z} - p_{v_i,z}) \left(\frac{eB}{2\pi} \right) \int_0^\infty d\rho \rho \times \int_0^{2\pi} d\phi e^{i\bar{v}_\perp \cdot \bar{x}_\perp} e^{i(N_{p_f} - R_{p_f})\phi} e^{-i(N_{p_i} - R_{p_i})\phi} I_{R_{p_i}, N_{p_i}}(\xi) I_{R_{p_f}, N_{p_f}}(\xi) \bar{U}_{p_f} \gamma_\mu (C_V - C_A \gamma_5) U_{p_i} \bar{U}_{\nu_f} \gamma^\mu (1 - \gamma_5) U_{\nu_i}, \quad (40)$$

where $\bar{v}_\perp = (p_{v_i,x} - p_{v_f,x})\hat{i} + (p_{v_i,y} - p_{v_f,y})\hat{j}$ and $\bar{x}_\perp = x\hat{i} + y\hat{j}$. To square the modulus of this expression we employ the properties

$$\begin{aligned} \delta^2(E_{p_f} + |p_{v_f}| - E_{p_i} - |p_{v_i}|) &= \delta(E_{p_f} + |p_{v_f}| - E_{p_i} - |p_{v_i}|) \frac{\mathcal{T}}{2\pi}, \\ \delta^2(p_{p_f,z} + p_{v_f,z} - p_{p_i,z} - p_{v_i,z}) &= \delta(p_{p_f,z} + p_{v_f,z} - p_{p_i,z} - p_{v_i,z}) \frac{L}{2\pi}. \end{aligned} \quad (41)$$

The transition rate is written as

$$\mathcal{W}_{fi}^{\text{prot}} = \frac{(2\pi)^2}{LV^2} \delta(E_{p_f} + |p_{v_f}| - E_{p_i} - |p_{v_i}|) \delta(p_{p_f,z} + p_{v_f,z} - p_{p_i,z} - p_{v_i,z}) |M_{fi}^{\text{prot}}|^2, \quad (42)$$

where we define

$$\begin{aligned} |M_{fi}^{\text{prot}}|^2 &= \frac{G_F^2}{2} \left(\frac{eB}{2\pi} \right)^2 \left| \int_0^\infty d\rho \rho \int_0^{2\pi} d\phi e^{i\bar{v}_\perp \cdot \bar{x}_\perp} e^{i(N_{p_f} - R_{p_f})\phi} e^{-i(N_{p_i} - R_{p_i})\phi} \right. \\ &\quad \left. \times I_{R_{p_i}, N_{p_i}}(\xi) I_{R_{p_f}, N_{p_f}}(\xi) \bar{U}_{p_f} \gamma_\mu (C_V - C_A \gamma_5) U_{p_i} \bar{U}_{\nu_f} \gamma^\mu (1 - \gamma_5) U_{\nu_i} \right|^2. \end{aligned} \quad (43)$$

The integration over the cylindrical coordinates ρ and ϕ can be done using relations (4.6) and (4.7) from Chap. II in Ref. [68]:

$$\int_0^{2\pi} \frac{d\phi}{2\pi} e^{i\bar{v}_\perp \cdot \bar{x}_\perp} e^{i(N_{p_f} - R_{p_f})\phi} e^{-i(N_{p_i} - R_{p_i})\phi} = J_{N_{p_f} - R_{p_f} - (N_{p_i} - R_{p_i})}(v_\perp \rho), \quad (44)$$

where $J_n(x)$ is the n th Bessel function and

$$\int_0^\infty d\rho \rho I_{R_{p_i}, N_{p_i}}(\xi) I_{R_{p_f}, N_{p_f}}(\xi) J_{N_{p_f} - R_{p_f} - (N_{p_i} - R_{p_i})}(v_\perp \rho) = \frac{1}{eB} I_{N_{p_i}, N_{p_f}}(\omega_\perp) I_{R_{p_i}, R_{p_f}}(\omega_\perp), \quad (45)$$

where $\omega_{\perp} = v_{\perp}^2/2eB$. Using these integrals, Eq. (43) is given by

$$|M_{fi}^{\text{prot}}|^2 = \frac{G_F^2}{2} I_{N_{p_i}, N_{p_f}}^2(\omega_{\perp}) I_{R_{p_i}, R_{p_f}}^2(\omega_{\perp}) |\bar{U}_{p_f} \gamma_{\mu} (C_V - C_A \gamma_5) U_{p_i} \bar{U}_{\nu_f} \gamma^{\mu} (1 - \gamma_5) U_{\nu_i}|^2. \quad (46)$$

With this expression we evaluate $\mathcal{W}_{fi}^{\text{prot}}$ in Eq. (42). Before we show an explicit expression for the total cross section, it is convenient to show the phase-space summations for protons and neutrinos:

$$\int d\Pi_p = \sum_{N_p=0}^{N_{p,\text{max}}} \sum_{R_p=0}^{R_{p,\text{max}}} \sum_{s_p=\pm 1} \frac{L}{2\pi} \int_{-\infty}^{\infty} dp_{p,z}, \quad (47)$$

$$\int d\Pi_{\nu_f} = \frac{V}{(2\pi)^3} \int d^3 p_{\nu_f}. \quad (48)$$

The value for $R_{p,\text{max}} = eBA/2\pi$, while $N_{p,\text{max}}$ is determined by the energy conservation: we fix the energy of the incident neutrino and the function $f(E_{s_{p_i}}, \mu_p, T)$ limits the maximum value for energy of the incident proton, which also limits $N_{p_i,\text{max}}$. Once the initial energy has a maximum value, so do $N_{p_f,\text{max}}$ and $N_{e_f,\text{max}}$ (see Appendix B in Ref. [54]). Now, the total scattering proton cross section is

$$\begin{aligned} \frac{\sigma_{\text{protscatt}}(\vec{p}_{\nu_i})}{V} &= \frac{G_F^2}{2} \frac{(2\pi)^2}{LV^2} V \int \frac{d^3 p_{\nu_f}}{(2\pi)^3} \sum_{N_{p_f}=0}^{N_{p_f,\text{max}}} \sum_{R_{p_f}=0}^{R_{p_f,\text{max}}} \sum_{s_{p_f}=\pm 1} \frac{L}{2\pi} \int_{-\infty}^{\infty} dp_{p_f,z} \sum_{N_{p_i}=0}^{N_{p_i,\text{max}}} \sum_{R_{p_i}=0}^{R_{p_i,\text{max}}} \sum_{s_{p_i}=\pm 1} \frac{L}{2\pi} \int_{-\infty}^{\infty} dp_{p_i,z} \\ &\times \delta(E_{p_f} + |p_{\nu_f}| - E_{p_i} - |p_{\nu_i}|) \delta(p_{p_f,z} + p_{\nu_f,z} - p_{p_i,z} - p_{\nu_i,z}) [1 - f(E_{s_{p_f}}, \mu_p, T)] f(E_{s_{p_i}}, \mu_p, T) \\ &\times I_{N_{p_i}, N_{p_f}}^2(\omega_{\perp}) I_{R_{p_i}, R_{p_f}}^2(\omega_{\perp}) |\bar{U}_{p_f} \gamma_{\mu} (C_V - C_A \gamma_5) U_{p_i} \bar{U}_{\nu_f} \gamma^{\mu} (1 - \gamma_5) U_{\nu_i}|^2. \end{aligned} \quad (49)$$

In this expression all the R_{p_i} and R_{p_f} dependence is in the function $I_{R_{p_i}, R_{p_f}}^2$. From Eq. (11.7) in Ref. [68], we have

$$\sum_{R_{p_i}=0}^{R_{p_i,\text{max}}} \sum_{R_{p_f}=0}^{R_{p_f,\text{max}}} I_{R_{p_i}, R_{p_f}}^2 = \sum_{R_{p_i}=0}^{R_{\text{max}}} 1 = R_{\text{max}} = \mathcal{A} \frac{eB}{2\pi}, \quad (50)$$

where $R_{p_i,\text{max}} = R_{p_f,\text{max}} = R_{\text{max}}$ is discussed in Appendix A in Ref. [54]. We define the proton structure function as

$$\begin{aligned} S_{s_{p_i}, s_{p_f}, N_{p_i}, N_{p_f}}^{\text{prot}} &= \int_{-\infty}^{\infty} \frac{dp_{p_i,z}}{2\pi} \int_{-\infty}^{\infty} \frac{dp_{p_f,z}}{2\pi} (2\pi)^2 \delta(E_{s_{p_f}} + |p_{\nu_f}| - E_{s_{p_i}} - |p_{\nu_i}|) \\ &\times \delta(p_{p_f,z} + p_{\nu_f,z} - p_{p_i,z} - p_{\nu_i,z}) f(E_{s_{p_i}}, \mu_p, T) [1 - f(E_{s_{p_f}}, \mu_p, T)]. \end{aligned} \quad (51)$$

An analytical expression for this structure function is given in Appendix A. Furthermore, it is convenient to define the lepton and hadron tensors as

$$L^{\mu\alpha} = \bar{U}_{\nu_f} \gamma^{\mu} (1 - \gamma_5) U_{\nu_i} \bar{U}_{\nu_i} \gamma^{\alpha} (1 - \gamma_5) U_{\nu_f}, \quad (52)$$

$$H_{\mu\alpha} = \bar{U}_{p_f} \gamma_{\mu} (C_V - C_A \gamma_5) U_{p_i} \bar{U}_{p_i} \gamma_{\alpha} (C_V - C_A \gamma_5) U_{p_f}. \quad (53)$$

It is easy to check that

$$H_{\mu\alpha} L^{\mu\alpha} = |\bar{U}_{p_f} \gamma_{\mu} (C_V - C_A \gamma_5) U_{p_i} \bar{U}_{\nu_f} \gamma^{\mu} (1 - \gamma_5) U_{\nu_i}|^2. \quad (54)$$

By making all these replacements in Eq. (49), the following is obtained:

$$\frac{\sigma_{\text{protscatt}}(\vec{p}_{\nu_i})}{V} = \frac{G_F^2}{2} \frac{eB}{2\pi} \int \frac{d^3 p_{\nu_f}}{(2\pi)^3} \sum_{N_{p_f}=0}^{N_{p_f,\text{max}}} \sum_{s_{p_f}=\pm 1} \sum_{N_{p_i}=0}^{N_{p_i,\text{max}}} \sum_{s_{p_i}=\pm 1} I_{N_{p_i}, N_{p_f}}^2(\omega_{\perp}) S_{s_{p_i}, s_{p_f}, N_{p_i}, N_{p_f}}^{\text{prot}} H_{\mu\alpha} L^{\mu\alpha}. \quad (55)$$

We replace now the initial proton spin wave function from Eq. (33),

$$\begin{aligned} \frac{\sigma_{\text{protscatt}}(\vec{p}_{\nu_i})}{V} &= \frac{G_F^2}{2} \frac{eB}{2\pi} \int \frac{d^3 p_{\nu_f}}{(2\pi)^3} \sum_{N_{p_f}=0}^{N_{p_f,\text{max}}} \sum_{s_{p_f}=\pm 1} \sum_{N_{p_i}=0}^{N_{p_i,\text{max}}} I_{N_{p_i}, N_{p_f}}^2(\omega_{\perp}) \\ &\times \left[\left(\frac{1 + A_{\text{prot}}}{2} \right) S_{s_i=1, s_{p_f}, N_{p_i}, N_{p_f}}^{\text{prot}} H_{\mu\alpha} L^{\mu\alpha} |_{s_i=1, s_f} + \left(\frac{1 - A_{\text{prot}}}{2} \right) S_{s_i=-1, s_{p_f}, N_{p_i}, N_{p_f}}^{\text{prot}} H_{\mu\alpha} L^{\mu\alpha} |_{s_i=-1, s_f} \right]. \end{aligned} \quad (56)$$

Finally for this section, we show the explicit expression for the contraction of the leptonic and hadronic tensors,

$$\begin{aligned}
H_{\mu\alpha}L^{\mu\alpha} = & C_V^2(1 + s_{p_i}s_{p_f})(1 + \cos\theta_{v_f}\cos\theta_{v_i} + \sin\theta_{v_f}\sin\theta_{v_i}\cos\phi_{v_f}) + C_A^2[3 - \cos\theta_{v_f}\cos\theta_{v_i} \\
& - \sin\theta_{v_f}\sin\theta_{v_i}\cos\phi_{v_f} - s_{p_i}s_{p_f}(1 - 3\cos\theta_{v_f}\cos\theta_{v_i} + \sin\theta_{v_f}\sin\theta_{v_i}\cos\phi_{v_f}) + 2(s_{p_i} - s_{p_f})(\cos\theta_{v_i} - \cos\theta_{v_f})] \\
& + 2C_AC_V(s_{p_f} + s_{p_i})(\cos\theta_{v_i} + \cos\theta_{v_f}).
\end{aligned} \tag{57}$$

In this expression we have employed spherical angles, where as mentioned we choose the z axis in the direction of the magnetic field. The θ angle uses this axis, while for the azimuthal angle we arbitrarily choose $\phi_{v_i} = 0$ and then ϕ_{v_f} is the azimuthal angle between the ingoing and outgoing neutrino. In Appendix B we discuss the limit of Eq. (56) for $B = 0$.

III. RESULTS AND DISCUSSION

In this section we present and discuss our results for the NMFP in homogeneous hot proto–neutron star matter under the presence of a strong magnetic field. We consider a range of densities $0.04 \leq \rho \leq 0.4 \text{ fm}^{-3}$, corresponding approximately to the outer core region of a neutron star, temperatures up to $T = 30 \text{ MeV}$, two intensities for the magnetic field ($B = 10^{17}$ and 10^{18} G), and different values for the proton fraction, ranging from symmetric matter ($N = Z$) up to pure neutron matter. The EOS is evaluated within the Hartree-Fock model, using LNS Skyrme interaction developed by Cao *et al.* [55]. The choice of this interaction is for two reasons. In the first place, in Ref. [53] we studied the inelastic scattering of neutrinos by neutrons, where we employed the same Skyrme model and the Brueckner-Hartree-Fock (BHF) approach using the Argonne V18 [69] nucleon-nucleon potential supplemented with the Urbana IX [70] three-nucleon force, having obtained a good agreement between both models. It is worth mentioning that the LNS Skyrme interaction is especially suitable for a comparison with the BHF model, since its parameters were determined by fitting the nuclear matter EOS calculated in the BHF framework. The second point refers to the effective mass predicted by the Skyrme model. Some Skyrme parametrization predicts small effective masses for high densities, which leads to a nonphysical increase of the NMFP. Effective masses evaluated using the LNS Skyrme interaction do not have this problem and we find that this parametrization is the most suitable for our problem.

As already mentioned, in this work we performed a self-consistent calculation of the NMFP. We start with the EOS for hot polarized proto–neutron star matter and then, using the single-particle energies, the chemical potentials, and the spin asymmetries from the EOS, we evaluate the NMFP. The spin asymmetries A_p and A_n are important quantities because they allow us to quantify the degree of polarization of the system. These quantities are evaluated from the EOS according to Eqs. (9), (12), and (15). The spin asymmetries appear explicitly in the cross-section reaction [see, for instance, Eq. (56)]. Also the single-particle energies and chemical potential are needed in the evaluation of the cross section, through the structure function as shown in Eq. (51). In Ref. [54] we showed that for the absorption reaction, the main source of asymmetry is not the A_n contribution in the initial spin wave

function, but the one from the structure function. Owing to this finding, we understand that it is important to perform a self-consistent treatment.

In the first place we discuss our results for the spin asymmetries A_p and A_n . A similar analysis was done in Ref. [56], but for a different interaction and for other conditions. The behavior of spin asymmetries can be understood through the interaction between three elements:

- (i) The direct coupling of particles with the magnetic field. For very low densities, this would lead to $A_p = 1$ and $A_n = -1$.
- (ii) The Pauli exclusion principle, which favors the condition $A_p = A_n = 0$. Clearly, we are solving the EOS and, in the absence of a magnetic field, the minimum of the energy configuration is the one which populates equally the levels with spin up and down.
- (iii) The nuclear interaction. While the behavior of the first two points is simple, this last element is more difficult. Based on the first two points, one expects that the magnitude of the spin asymmetries starts with a maximum at low density, and decreases monotonously as the density grows. As we soon see, the inclusion of the nuclear interaction could alter this pattern.

In Fig. 1, we study the instability construction for the spin asymmetry as shown in Eq. (27). We consider the condition $B = 10^{18} \text{ G}$, $T = 5 \text{ MeV}$, with two values for the spin asymmetry $\omega = 0$ and 0.5 . The value $\omega = 0$ at $T = 5 \text{ MeV}$ is an extreme condition for the instability (it is solved using the Maxwell construction), whereas $\omega = 0.5$ at the same temperature represents an intermediate situation which allows us to discuss the Gibbs construction. The system becomes unstable due to the nuclear interaction among protons and neutrons. This takes place for low densities and temperatures, with or without a magnetic field. When the proton fraction decreases, so does the instability region, which is absent for pure neutron matter. We have organized this figure into two columns: the first one for $\omega = 0$ and the second one for $\omega = 0.5$. The finite density region of the instability starts very close to the origin and it has not been drawn; by a vertical dotted line (in all panels) we show the upper limit for the instability. In the first row [Figs. 1(a) and 1(b)], we show α as a function of the baryonic density. In Fig. 1(a) we have $\omega = 0$. In this case, α is a linear function of the density as discussed in Sec. II B. Figure 1(b) is evaluated using the Gibbs construction and exhibits a similar behavior as in Fig. 1(a), but it is no longer a linear function. To understand the instability construction in Eq. (27), in Figs. 1(c) and 1(d), we depict W_p and W_n (we recall that $W_i = \rho_{i,s_i=1} - \rho_{i,s_i=-1}$). We employed a continuous (dash-dotted) line for the asymmetries with (without) the instability construction. In Fig. 1(c), there are four horizontal dashed lines

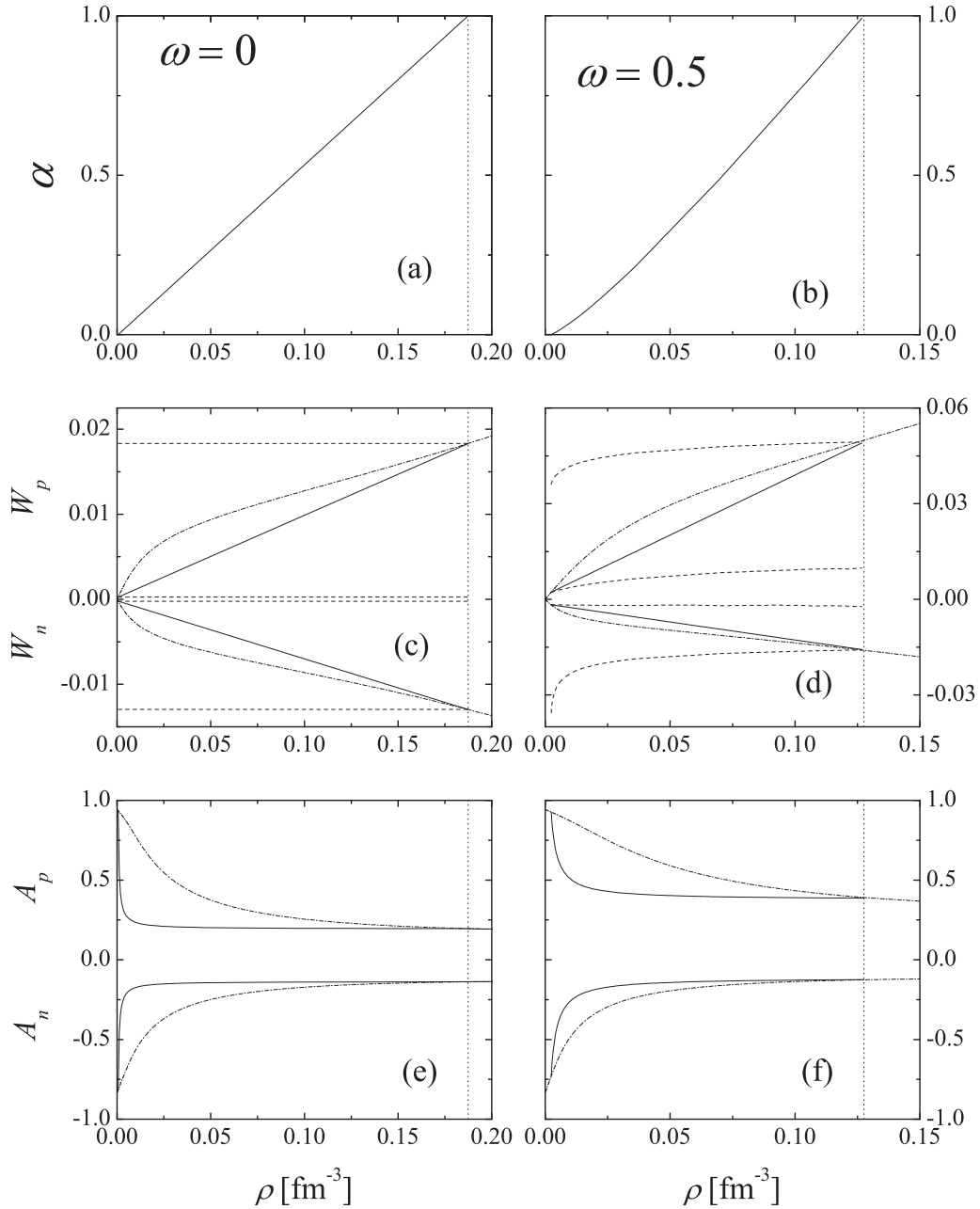


FIG. 1. The spin asymmetry with and without the instability construction for both protons and neutrons. The magnetic field intensity is $B = 10^{18}$ G, $T = 5$ MeV, and we consider two values of the isospin asymmetry ω . [(a), (b)] The parameter α [see Eq. (21)]. [(c), (d)] The continuous line is the final result for W_n and W_p , while the dash-dotted line is the result without the instability construction. In these same panels we have plotted W_i^a and W_i^b by dashed lines. The final value for W_i is obtained with α and these quantities using Eq. (27). Finally, in (e) and (f), we have A_n and A_p , where the continuous (dash-dotted) lines include (do not include) the instability construction. In all panels a vertical dotted line indicates the upper limit of the instability. The lower limit is very close to the origin and it is not shown. Units for W_i are fm^{-3} .

representing the constant values for W_p^a and W_p^b (positives) and W_n^a and W_n^b (negatives). From Eq. (27), the final result for W_i starts at W_i^a in the lower limit of the instability and ends at W_i^b . In Fig. 1(d) we have $\omega = 0.5$ and in this case α , W_i^a , and W_i^b are all functions of the density. Beyond this density dependence, the construction is the same as in Fig. 1(c). In Figs. 1(e) and 1(f), we give the final values for A_p and A_n , with and without the instability construction. We notice that

the existence of two phases significantly reduces the degree of polarization, due to the admixture with a higher density and weaker polarization state, resulting from the equilibrium conditions of the EOS. In what follows we present results for other temperatures and isospin asymmetries. The change from the extreme conditions in this figure up to the disappearance of the instability is continuous. Except for $\omega = 0$ and as long as there is an instability, the two coexisting phases have a

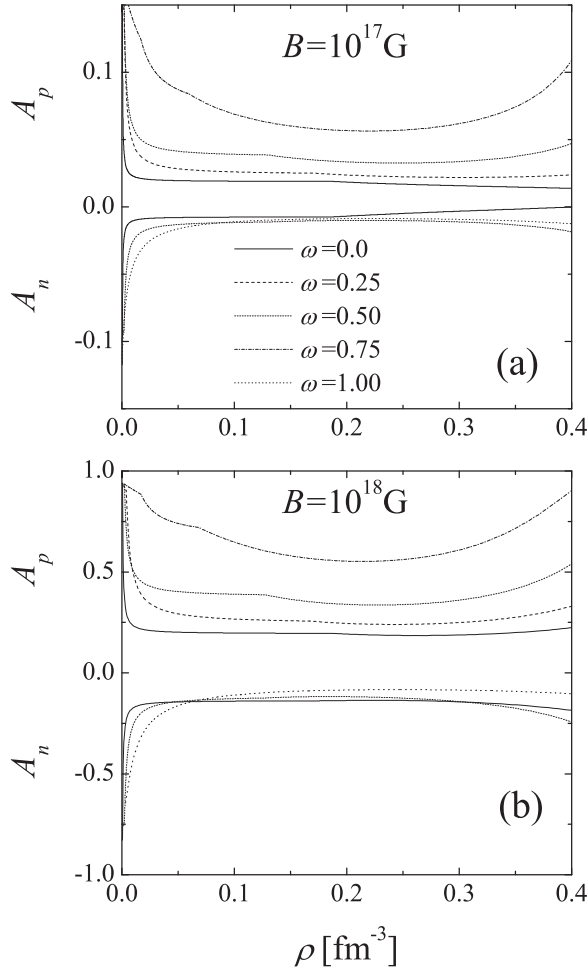


FIG. 2. Density dependence of the proton and neutron spin asymmetries for $T = 5$ MeV, as defined in Eq. (15). The magnetic field is (a) $B = 10^{17}$ and (b) $B = 10^{18}$. Both panels give results for different values of the isospin asymmetry ω . In this figure the Gibbs or Maxwell construction has been already implemented.

different density, spin, and isospin asymmetries, subject to the constraints in Eqs. (19) and (20). But the effects of these changes are not significant over the NMFP, as we show soon.

In Fig. 2, we present our results for A_p and A_n as a function of the total baryonic density for two values of the magnetic field and for different isospin asymmetries. These results take care of the instability construction. By comparison between Figs. 2(a) and 2(b), the spin asymmetry decreases in magnitude for decreasing values of the magnetic field intensity. Beyond this point, in this figure we want to study the dependence of A_p and A_n with the proton fraction. Values of these quantities are given from symmetric matter ($\omega = 0$), where the numbers of protons and neutrons are the same, up to pure neutron matter ($\omega = 1$, where A_p is absent). Owing to the scale of the figure and to avoid confusion, for A_n we omitted the intermediate values $\omega = 0.25$ and 0.75 . Our results are consistent with those in Ref. [56], which correspond to a different nuclear interaction. The overall behavior shows a stronger dependence with the proton fraction for A_p . This results from the stronger coupling of protons with

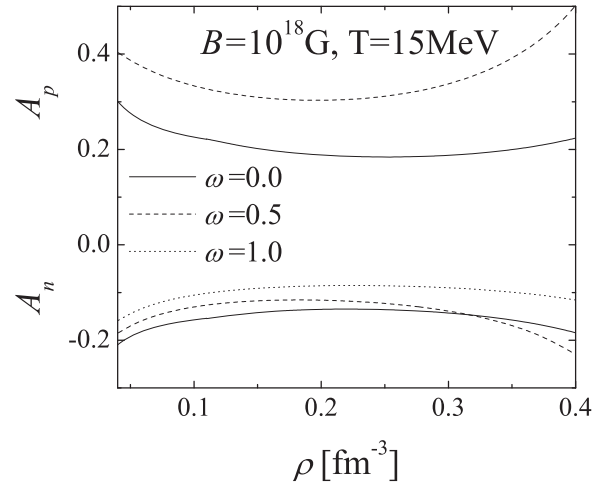


FIG. 3. Proton and neutron spin asymmetries for different values of the isospin asymmetry.

the magnetic field than the one for neutrons. In this figure, we can analyze three baryonic density regions: low densities, medium densities, and high densities. For medium densities we notice that the magnitude of A_n decreases for increasing values of ω , while the inverse situation takes place for A_p . As ω grows, the proton fraction decreases. That is, an increase in the relative density of neutrons reduces its polarization. Alternatively, a lower density of protons favors higher values for A_p . For higher densities the increase of the polarization is a particular result for the Skyrme model due to its ferromagnetic instability.

For further use, in Fig. 3 we plotted the spin asymmetries A_p and A_n within the density region of interest to us, for $B = 10^{18}$ G, $T = 15$ MeV, and $\omega = 0, 0.5$, and 1 . For this temperature the spin asymmetry is more important for A_p , even for $\omega = 0$. This is more noticeable for low densities, but is also present for intermediate ones. For $\omega = 0.5$, we have that A_p is much bigger than $|A_n|$, as the spin asymmetry grows for lower partial densities. For this temperature, the instability is only present for $\omega = 0$, but it is almost negligible.

The effect of the temperature over the spin asymmetries is shown in Fig. 4, for two different isospin asymmetries: $\omega = 0$ and 0.5 . As expected, an increase in temperature decreases the magnitude of spin asymmetries, since this increase favors spin disorder. However, for a certain low-density region the depolarization due to the two coexisting phases at $T = 5$ MeV is more important than the thermal effect. In Fig. 4(a) we show our results for symmetric matter, where both $|A_p|$ and $|A_n|$ exhibit the same behavior. In this case, for low densities the depolarization at $T = 5$ MeV due to the coexistence of two phases is more important than the thermal depolarization at $T = 15$ MeV. The same happens for A_n for $\omega = 0.5$ [Fig. 4(b)]. But for A_p also for $\omega = 0.5$, the situation is no longer symmetric and except for a few points the thermal effect is more important. Moreover, the split among different temperatures increases significantly for A_p . The reason is simply because for $\omega = 0.5$ the proton density is smaller and thermal effects are more important.

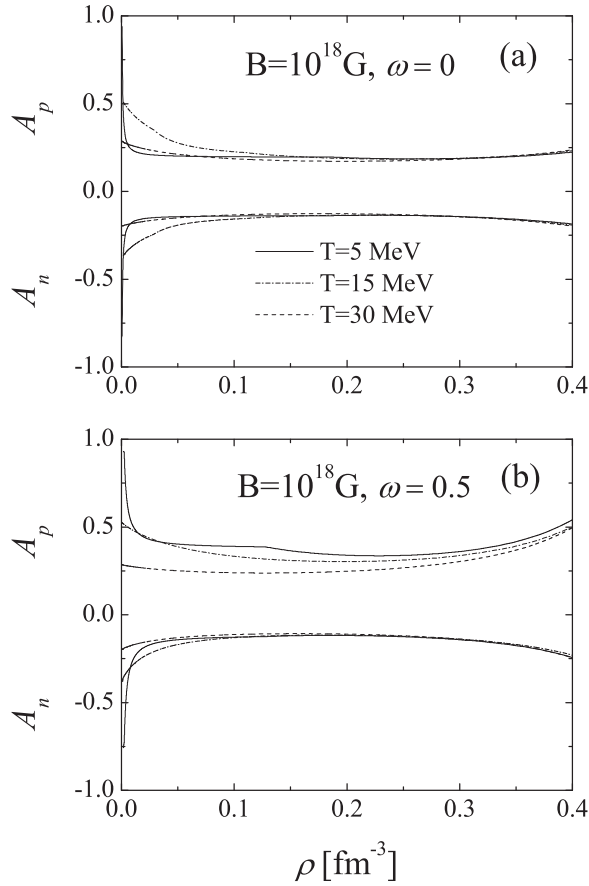


FIG. 4. Density dependence of the proton and neutron spin asymmetries for different temperatures and for two isospin asymmetries. Only for $T = 5$ MeV the instability construction shows a sizable effect.

We turn now to the NMFP. We recall that we consider three reactions: (i) the neutron inelastic scattering $\nu_i + n_i \rightarrow \nu_f + n_f$, (ii) the proton inelastic scattering $\nu_i + p_i \rightarrow \nu_f + p_f$, and (iii) the neutrino absorption $\nu_i + n_i \rightarrow e_f^- + p_f$. Reactions (i) and (iii) were studied for pure neutron matter in Refs. [53] and [54], respectively. The employment of proto-neutron star matter requires some further analysis for these reactions, which we will consider soon. We start by discussing the neutrino-proton scattering reaction. To the best of our knowledge, this reaction has not been discussed yet within proto-neutron star matter with a strong magnetic field in a self-consistent way. In doing so, we will compare with previous results for the neutron scattering and neutrino absorption reactions, particularly the ones in Fig. 11 in Ref. [53] and in Fig. 6 in Ref. [54]. This is only a qualitative comparison, as those works use pure neutron matter.

In Fig. 5, we present our result for the neutrino-proton scattering NMFP as a function of the density, at a temperature $T = 15$ MeV, for two values of the magnetic field $B = 10^{17}$ G and $B = 10^{18}$ G, an isospin asymmetry $\omega = 0.5$ and for three different angles of the incoming neutrino. In the first place, the NMFP decreases for increasing values of the magnetic field intensity. Let us focus on the $\theta_\nu = \pi/2$ case. For this angle and for the neutron scattering reaction, the result is almost

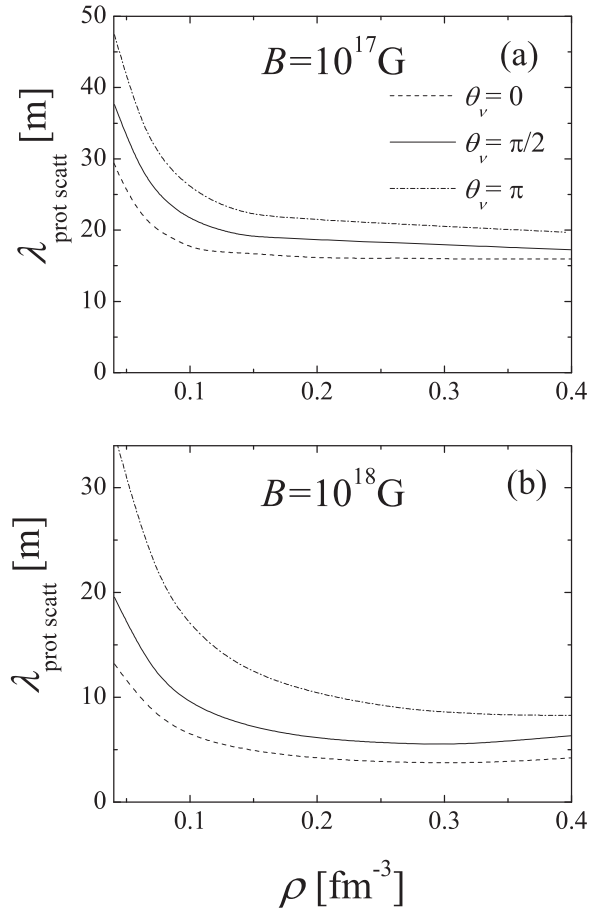


FIG. 5. The proton scattering NMFP as a function of the density and for three different values for the neutrino incoming angle, θ_ν . Results for a magnetic field intensity (a) $B = 10^{17}$ G and (b) $B = 10^{18}$ G. For both panels, the momentum of the incoming neutrino is $|\vec{p}_\nu| = 3T$, $T = 15$ MeV, and $\omega = 0.5$.

independent of B . For the proton scattering and absorption reactions the situation is different: having charge particles the Landau quantization comes into play. From $B = 10^{17}$ G to $B = 10^{18}$ G there is a reduction in the NMFP. As in the case of the absorption reaction, for proton scattering the number of possible Landau final states decreases as B grows. However, the degeneracy of the levels is given by a factor $eBA/2\pi$ [71]. This increasing degeneracy factor competes with the reduction of Landau levels and from the numerical analysis it results in a reduction for the NMFP, similar to the case of the absorption reaction.

Continuing with the analysis of Fig. 5, we now study the results for the three angles $\theta_\nu = 0, \pi/2, \pi$. In the first place, neutrinos are more transparent to polarized proto-neutron star matter when moving in a direction antiparallel to the magnetic field ($\theta_\nu = \pi$). The situation is the opposite of the one for the absorption and neutron scattering. This is easily understood due to the coupling of the proton with the magnetic field, which is already present in the different sign between A_p and A_n . Therefore, while the asymmetry induced by the magnetic field favors a bigger flux of neutrinos antiparallel to the magnetic field for the proton scattering reaction, the opposite

happens for the two remaining reactions. But perhaps the most striking point is the degree of reduction in the asymmetry in the NMFP from $B = 10^{18}$ G to $B = 10^{17}$ G, which can be defined as the difference between the mean free paths for the extreme values $\theta_\nu = 0$ and $\theta_\nu = \pi$ [an analytical expression is given in Eq. (59)]. For the same reduction in the magnetic field strength, the decrease in the mean free path asymmetry is much more pronounced for the absorption and the neutron scattering reactions. In a certain way, we could anticipate this result by the values of the spin asymmetries in Fig. 3: for $\omega = 0.5$ we have $|A_p| \approx 2|A_n|$. This single point is not enough to understand the different rate in the reduction of the mean free path asymmetries. To get a better understanding of the problem, we can consider three elements which are responsible for the asymmetry in the NMFP: (1) the spin asymmetry in the initial wave function as shown in Eq. (33), where A_i appears explicitly; (2) the structure function [Eq. (51)], which depends on the single particle energies and chemical potential from the EOS; and (3) the weak interaction transition matrix element in Eq. (43), which has a spin dependence. Obviously the combined effect of all these elements leads to the final result. From the numerical analysis it turns out that it is the way in which the structure functions weight the different weak terms in Eq. (56), the main effect which explains the behavior for the proton-scattering reaction. This significant difference between the reduction rate among the different reactions emphasizes the need for performing a self-consistent treatment of the problem.

In Fig. 6 we consider the effect of the temperature over the proton scattering NMFP. We show results for the NMFP for temperatures $T = 5, 15,$ and 30 MeV, for two values of the magnetic field, $\omega = 0.5$ and $\theta_\nu = \pi/2$. There is a strong dependence of the NMFP on the temperature, where the NMFP decreases for increasing values of temperature. This qualitative behavior is a common feature of all mean free paths: as temperatures increase, so does the available phase space of final states. However, while this dependence is weak for the absorption reaction, both proton and neutron scattering reactions show a strong dependence. Also in this figure we have evaluated the instability construction, only needed for $T = 5$ MeV, which can be noticed at low densities. In the next figure we analyze in detail the effect of the instability construction.

To analyze the effect of the instability construction over the NMFP, we now consider the three reactions discussed in this work. This is done in Fig. 7, where we set $B = 10^{18}$ G, $\omega = 0$, and $T = 5$ MeV. We have chosen these values for the isospin asymmetry and temperature because they are the values for which the instability construction is most important. The effect of the instability construction over the mean free path for each reaction is rather similar. Note that the initial and final densities which determine the instability region come from the EOS and are common to any reaction mechanism. We show results for the NMFP starting at $\rho = 0.04 \text{ fm}^{-3}$. For lower densities the NMFP takes big values which would mask the results within the density region of interest. But to build up the instability construction the starting density is very small. More specifically the instability region for the conditions of these figures is $\rho \in [0.55 \times 10^{-3}, 0.187] \text{ fm}^{-3}$.

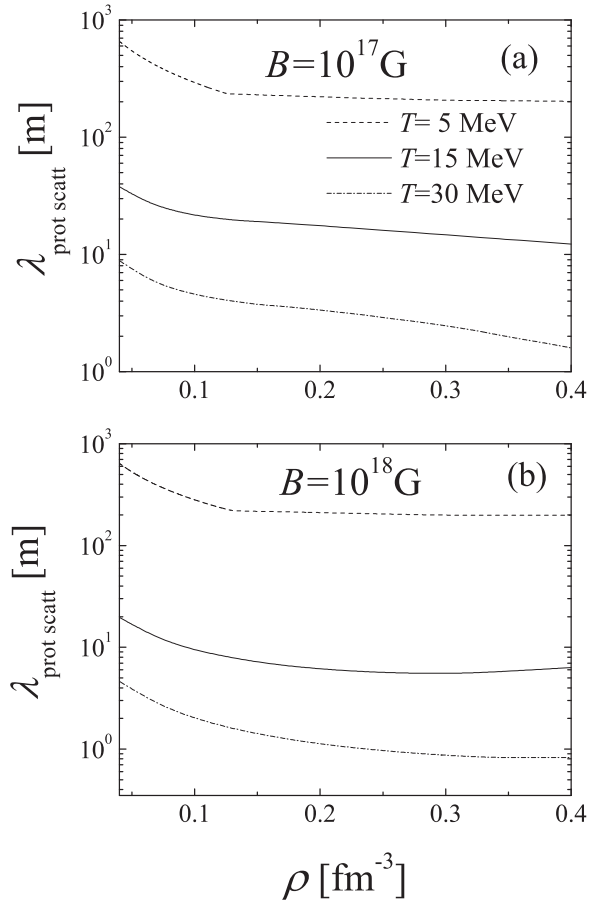


FIG. 6. The proton scattering NMFP as a function of the density and for three different values for the temperature for $\theta_\nu = \pi/2$ and $\omega = 0.5$. As in Fig. 3, results for a magnetic field intensity (a) $B = 10^{17}$ and (b) $B = 10^{18}$ G, respectively, using the same approximation for the momentum of the incoming neutrino.

In this figure we look at the results for three incoming angles: $\theta_\nu = 0, \pi/2,$ and π . The continuation of dotted lines is the result without the instability construction. One first conclusion from the instability construction is that it reduces the asymmetry in the NMFP. This is consistent with the results from the spin asymmetries in Fig. 1 (note that this figure starts at $\rho = 0$). Second, the instability construction reduces the importance of all the reactions, as it leads to a longer NMFP. This results from the instability construction in the same way as it was discussed in Fig. 1, but now the mean free path summation is given by Eq. (29). In what follows, the instability construction will be implemented wherever is necessary. For growing temperatures and for smaller proton fraction, it becomes less important and eventually it disappears. As mentioned, the instability originates from nuclear interaction and the instability region depends on the particular model for this interaction.

Before we discuss our final results for the total NMFP, in Fig. 8 we study the dependence of the neutrino mean path with the isospin asymmetry, starting from symmetric matter ($\omega = 0$ or $\rho_p = \rho_n = \rho/2$) to pure neutron matter ($\omega = 1$ or $\rho_p = 0$ and $\rho_n = \rho$), considering several intermediate values. In this

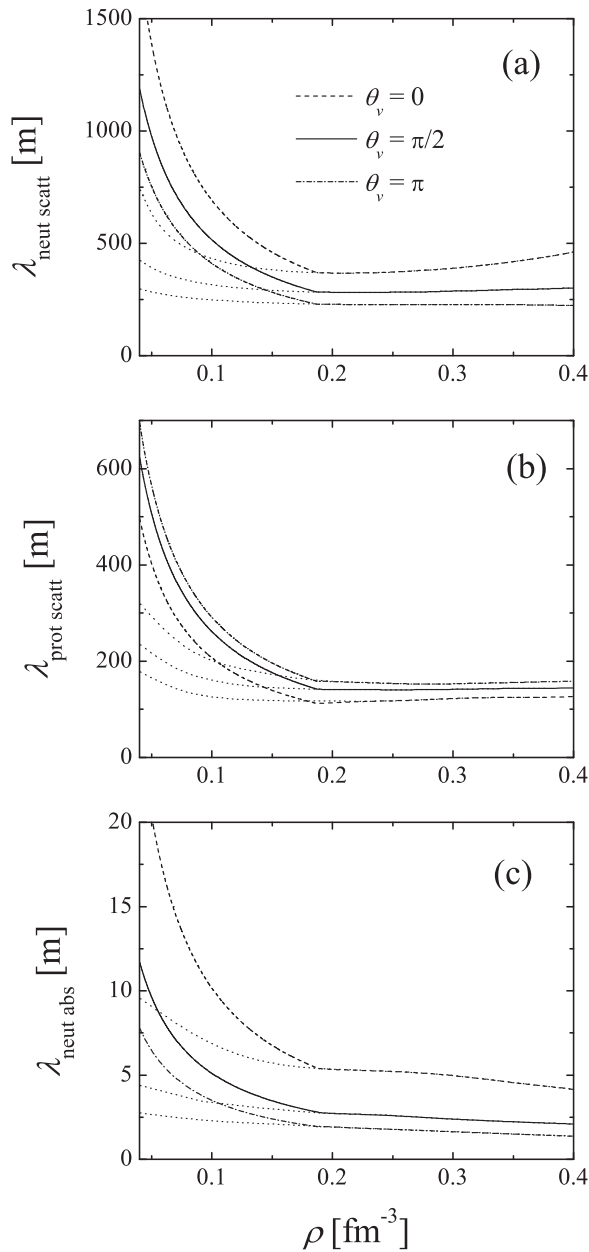


FIG. 7. Effect of the instability over the NMFP. In all curves the dotted lines represent the result without the instability construction. We have employed $B = 10^{18}$ G, $T = 5$ MeV, $\omega = 0$, and three values for the incoming neutrino angle θ_v . The momentum model for the incoming neutrino is the same as in Fig. 5.

figure we used $B = 10^{18}$ G and $T = 15$ MeV. Only for $\omega = 0$ do we have the instability construction, which is almost negligible. These results are easily understood because, for a given total baryonic density ρ and for an isospin asymmetry ω , the partial proton and neutron densities are $\rho_p = \rho(1 - \omega)/2$ and $\rho_n = \rho(1 + \omega)/2$, respectively. For the absorption and for the neutron scattering reaction, the neutrino interacts with a neutron, which means that these reactions are governed by ρ_n , while for the proton scattering the dependence is with ρ_p . For increasing values of ω and for a fixed ρ , we have that ρ_n increases, while ρ_p decreases. This means that the

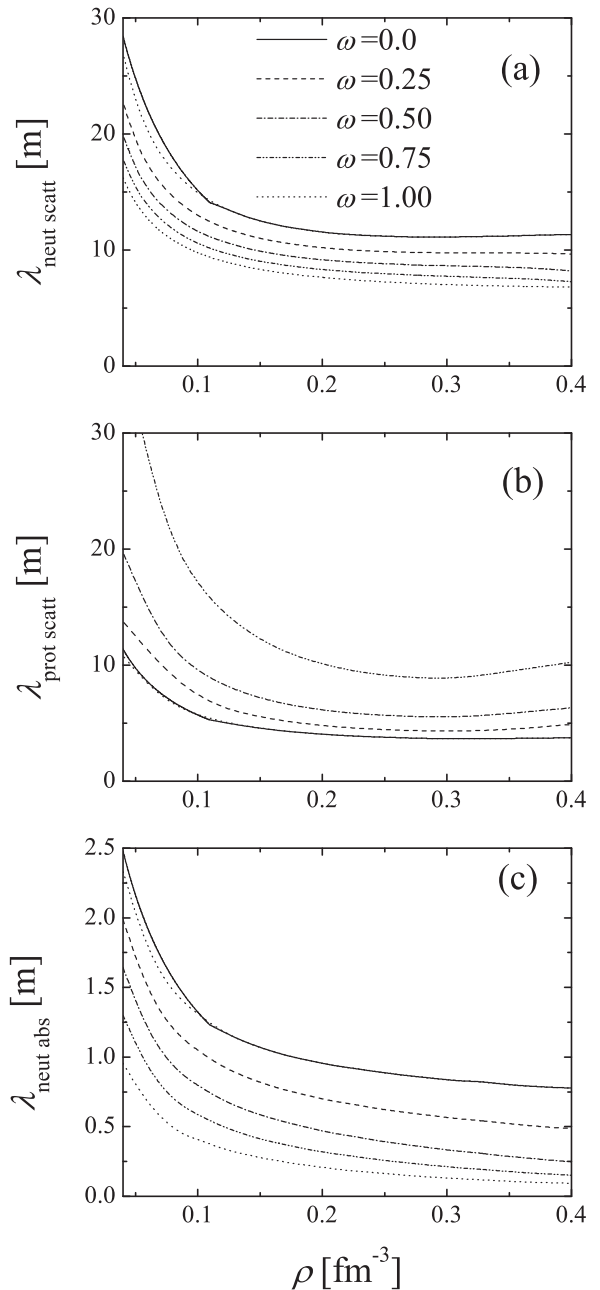


FIG. 8. The NMFP for different values of the isospin asymmetry ω . For $\omega = 0$ the curve is divided into a solid line and a dotted line, which represent the result with and without the instability construction, respectively. In this figure we have used $B = 10^{18}$ G and $T = 15$ MeV. For the incoming neutrino, we have employed $\theta_v = \pi/2$ and the same model for the momentum as in Fig. 5.

absorption and neutron scattering have an increasing partial density which reduces their mean free path, and the opposite occurs for the proton scattering reaction, which explains the results in this figure.

Finally, in Figs. 9 and 10, we present our results for the total NMFP, for $B = 10^{17}$ G and $B = 10^{18}$ G, respectively. We fix the temperature at $T = 15$ MeV and we show results for three isospin asymmetries: $\omega = 1, 0.5$, and 0 . The total

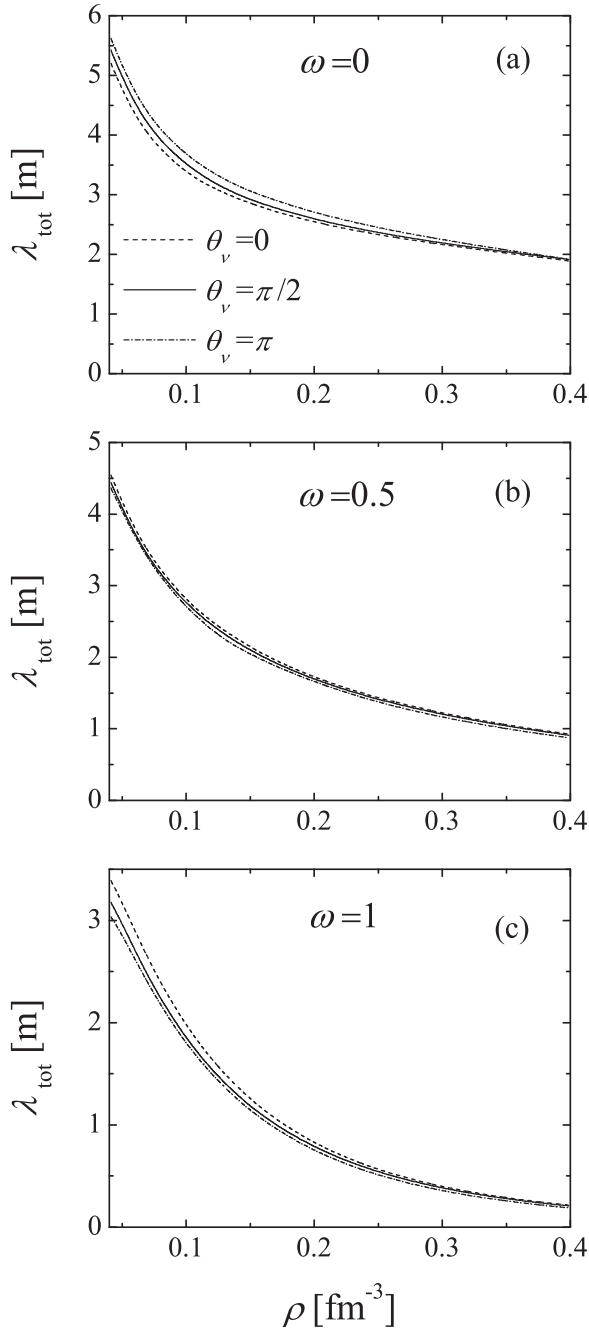


FIG. 9. The total NMFP for different values of the isospin asymmetry ω and for three different angles of the incident neutrino. In this figure we have used $B = 10^{17}$ G and $T = 15$ MeV. We have employed the same model for the momentum as in Fig. 5.

NMFP results from the addition of the mean free path for each reaction as

$$\lambda_{\text{tot}} = \left(\frac{1}{\lambda_{\text{neut scatt}}} + \frac{1}{\lambda_{\text{prot scatt}}} + \frac{1}{\lambda_{\text{neut abs}}} \right)^{-1}. \quad (58)$$

For convenience we first discuss Fig. 10. In this case the total NMFP is dominated by the absorption reaction. When moving from neutron matter to symmetric matter, the neutron compo-

nent of the medium decreases which results in an increase of the absorption mean free path, as seen in both Figs. 9 and 10. At this point, it is convenient to define the asymmetry of the NMFP as

$$A_\lambda \equiv \frac{\lambda_{\theta_v=0} - \lambda_{\theta_v=\pi}}{\lambda_{\theta_v=0} + \lambda_{\theta_v=\pi}}. \quad (59)$$

The aim of these figures is to discuss the dependence of the asymmetry in the mean free path with the proton fraction. Under the presence of a strong magnetic field, each contribution to the total NMFP has common features: λ increases for decreasing partial densities (ρ_n or ρ_p), but the opposite happens with A_λ —both λ and A_λ decrease for increasing temperatures. Obviously A_λ increases as the magnetic field grows. We recall that $\lambda_{\text{prot scatt}}$ ($\lambda_{\text{neutscatt}}$ and λ_{neutabs}) is sensitive to the partial proton (neutron) density. On the other hand, while $\lambda_{\text{neutscatt}}(\theta_v = \pi/2)$ is almost independent of the magnetic field intensity, both $\lambda_{\text{prot scatt}}$ and λ_{neutabs} decrease when the magnetic field is incremented. The degree of the dependence of each mean free path with these variables differs from one reaction to another.

Under the conditions of Fig. 10 and for $\omega \approx 0.5$, there is a quasicancellation among the asymmetries in the mean free path between $\lambda_{\text{prot scatt}}$ and $\lambda_{\text{neut scatt}}$. To be clear, $\lambda_{\text{prot scatt}}(\theta_v = \pi/2) \sim \lambda_{\text{neut scatt}}(\theta_v = \pi/2)$, $\lambda_{\text{prot scatt}}(\theta_v = \pi) \sim \lambda_{\text{neut scatt}}(\theta_v = 0)$, and $\lambda_{\text{prot scatt}}(\theta_v = 0) \sim \lambda_{\text{neut scatt}}(\theta_v = \pi)$. From the figure itself A_λ looks similar for all the isospin asymmetries. In Table I, we show explicit values for three representative densities. We see that for $B = 10^{18}$ G, A_λ take similar values. Unfortunately the Skyrme interaction shows an unphysical polarization at high densities. Beyond this point, A_λ is dominated by the absorption reaction as mentioned. Starting at $\omega = 1$, we observe an increase of A_λ at $\omega = 0.5$. This is because the scattering reactions are neutralized between each other and the decrease of the partial neutron density induces an increase of A_λ for the absorption reaction. From $\omega = 0.5$ to $\omega = 0$ the same happens for the absorption reaction, but now the partial density of protons is important and the asymmetry from the proton scattering reaction becomes more relevant and produces a small decrease in A_λ .

For Fig. 9, the general considerations discussed for Fig. 10 remain valid. As expected, the reduction in one order of magnitude for the magnetic field strongly reduces the split among the different θ_v components of the mean free path. This reduction is not uniform: it is very important for the neutron scattering and for the neutron absorption reactions, but it is weaker for the proton scattering reaction, as already discussed (see Fig. 5). In fact, for symmetric matter ($\omega = 0$) where the weight for the proton scattering reaction is maximum, A_λ changes its sign. This is more clearly seen in Table I. The conditions for which this change in sign takes place depend on the particular model and the nuclear interaction chosen for the calculation. However, the general behavior of each component must still be valid, and this change in sign is expected.

The presence of a strong magnetic field deeply modifies the NMFP. In the absence of a magnetic field and using an analogous nonrelativistic model (see, for instance, Ref. [40]), the analytical expressions for the three reactions considered

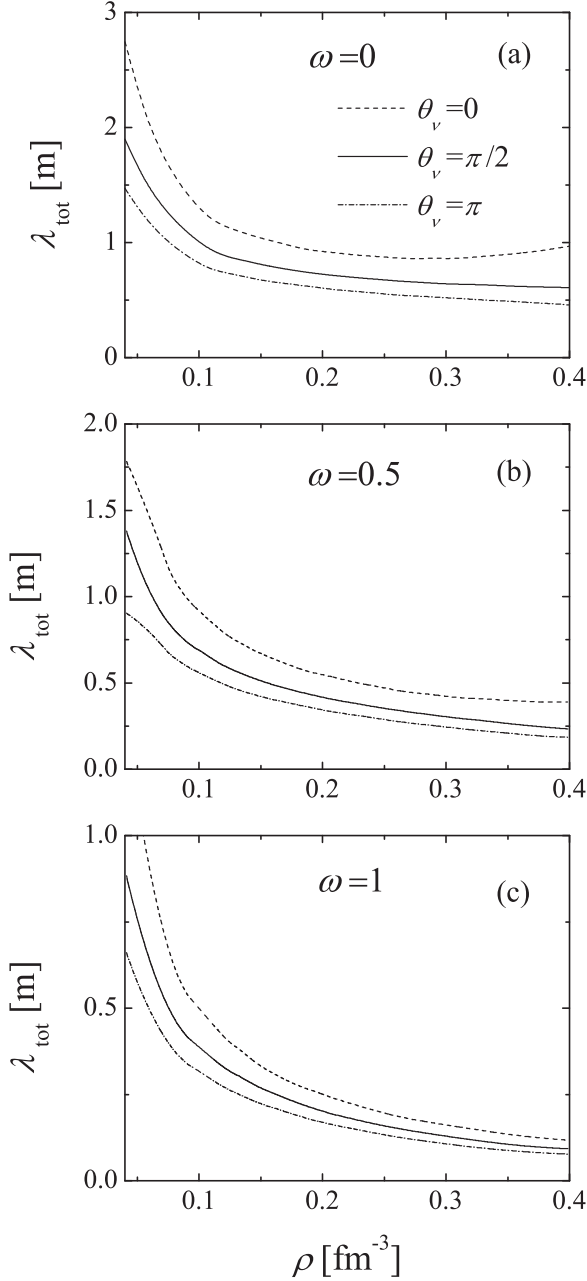


FIG. 10. The total NMFP for different values of the isospin asymmetry ω and for three different angles of the incident neutrino. In this figure we have used $B = 10^{18}$ G and $T = 15$ MeV. We have employed the same model for the momentum as in Fig. 5.

in this work are the same. Each reaction has its own coupling constants and from the EOS neutrons and protons have different values for their single-particle energies and chemical potentials. But the functional dependence on temperature and density is basically the same for all reactions. In the first place, the magnetic field modifies the EOS, leading to a partially polarized system. For the neutron scattering reaction, the NMFP for a neutrino incoming angle $\theta_\nu = \pi/2$ is very similar to the result for $B = 0$. The main sources of asymmetry in the neutron scattering mean free path are the initial spin wave

TABLE I. Some values for the asymmetry in the NMFP from Eq. (59). These asymmetries refers to λ_{tot} and correspond to the conditions in Figs. 9 and 10, for $B = 10^{17}$ G and $B = 10^{18}$ G, respectively.

B (G)	ρ (fm^{-3})	A_λ ($\omega = 1$)	A_λ ($\omega = 0.5$)	A_λ ($\omega = 0$)
10^{17}	0.08	0.048	0.015	-0.021
	0.16	0.047	0.022	-0.009
	0.32	0.060	0.025	-0.018
10^{18}	0.08	0.243	0.258	0.241
	0.16	0.191	0.227	0.211
	0.32	0.211	0.286	0.260

function shown in Eq. (33) and the weak interaction matrix element. The two remaining reactions involved charged particles for which the Landau quantization comes into play. For these reactions, there is a strong correlation between the strong interaction in the EOS and the weak interaction which leads to particular behaviors for each reaction. Obviously the proton fraction is in this case an important variable: having a different behavior for each reaction, the proton fraction alters the relative weight of each reaction. This is clearly reflected in the results from Fig. 9 contained in Table I.

In this work our main concern has been the asymmetry in the NMFP for hot proto-neutron star matter. In particular, we analyzed the dependence of this quantity on the proton fraction. Neutrinos play an important role in the cooling of neutron stars and, in the early stages of this compact object, the proton fraction can be important. A different approach would be to consider β -stable matter with charge neutrality. In this case, electrons must be considered both in the EOS and in the total NMFP. At present we are working on an EOS for this case [72]. Relativistic effects cannot be neglected for the electrons. For the EOS and neglecting the electromagnetic interaction with protons and between electrons, we take care of relativistic effects by proper choice of the single-particle energy. But the situation is more complex for the evaluation of the mean free path, because one has to employ relativistic structure functions. This point is discussed in the absence of magnetic fields by Horowitz and Wehrberger [36]. Also the electron neutrino inelastic scattering within a dense medium, at finite temperature, and for a strong magnetic field is discussed by Bezchastnov and Haensel [45]. In this work a fully relativistic formalism is developed for the electron neutrino differential cross section, but instead of developing an EOS, the authors take constant values for the electron chemical potential. Electrons play a role in the NMFP, but its inclusion using β -stable matter with charge neutrality is beyond the scope of this work.

Several works discuss the neutrino cross section or mean free path under the presence of a strong magnetic field and in Ref. [54] we give a brief overview of these works, which we do not repeat here. What differentiates ours from these works is the self-consistent treatment that we do, where we evaluate the EOS for the same conditions that we use later for the NMFP.

Before we end this section, it is worth commenting on some subjects where our scheme could be applied. To start

with, in this work we considered only neutrinos. A similar analysis can be performed for antineutrinos. In this case, we have the scattering reactions $\bar{\nu} + n \rightarrow \bar{\nu}' + n'$ and $\bar{\nu} + p \rightarrow \bar{\nu}' + p'$, together with the antineutrino absorption $\bar{\nu} + p \rightarrow e^+ + n$. In Ref. [4], for instance, the rates for the charged-current processes $\nu + n \rightleftharpoons e^- + p$ and $\bar{\nu} + p \rightleftharpoons e^+ + n$ are evaluated for a strong magnetic field and finite temperature. This calculation is done in free space. These rates are important for understanding the dynamics of supernova explosion (a related discussion on the dynamics of supernovas can be found in Ref. [5]) as well as the evolution of the proto-neutron star just after its formation [12–14]. In another work [6] (see also Ref. [7] for a review on the subject), the effect of neutrinos on the r -process nucleosynthesis is discussed: in the absorption reaction $\nu + n \rightarrow e^- + p$, the capture of a neutrino by a neutron produces a proton (and an electron). The produced protons rapidly form low-mass seed nuclei (especially α particles) for the r process. Clearly, there would be a competition with the antineutrino absorption reaction $\bar{\nu} + p \rightarrow e^+ + n$. However, in the referred work no magnetic field is considered and the effect of the medium on the NMFP is incorporated in an approximate way.

As a further comment on these charged-current reactions, it should be mentioned that there are several works which deal with this subject in the absence of magnetic fields (or using weak magnetism) [8–11]. All these works evaluate the (anti)neutrino rate in hot and dense matter in the mean field level. The employment of an EOS induces changes in the charged-current (anti)neutrino opacities which have important consequences for nucleosynthesis, flavor oscillations, and neutrino detection on Earth (for details see Ref. [8]). In Ref. [9] random phase approximation correlations are also included, weak magnetism is considered in Ref. [10], while charged currents with muons are discussed in Ref. [11]. The general conclusion from these works is that correlations are important for an accurate evaluation of charged-current reactions.

Similar calculations within our model are feasible, but they are not straightforward. In the first place, we have made a point on a self-consistent treatment of the EOS and the evaluation of the neutrino cross section. Therefore, to evaluate the rates, the EOS must contain electrons and positrons, a point which we briefly discussed above and certainly is a quite involved task when a strong magnetic field is present. In addition, the antineutrino weak matrix elements are different from the neutrino ones. It should be noted that the antineutrino results cannot be added to the neutrino ones. In particular, a model for the relative abundance of neutrinos and antineutrinos is required. In a rather arbitrary way, we can group the contributions just discussed into two sets: the ones which consider a strong magnetic field but no EOS, and the ones which employ an EOS without a strong magnetic field. The overall result is that both the EOS and the magnetic field induce significant changes in the charged-current processes. In the present work, we have shown that the relative importance of each contribution depends on the condition in which they were evaluated. From this, and without the inclusion of antineutrinos, we prefer not to draw any conclusion on the effect of the magnetic field over these astrophysical problems.

We understand that the model developed in this contribution is suitable for the inclusion of antineutrinos, together with the inverse reactions, once a more elaborated EOS is developed. However, and due to its complexity, we leave this analysis for a future work.

IV. SUMMARY AND CONCLUSIONS

In this work we evaluated the NMFP for hot proto-neutron star matter under a strong magnetic field. We considered densities in the range $0.04 \leq \rho \leq 0.4 \text{ fm}^{-3}$, temperatures of 5, 15, and 30 MeV, two magnetic field strengths $B = 10^{17}$ and 10^{18} G, and different proton fractions ranging from symmetric matter up to pure neutron matter. Due to the scale of the processes involved, we consider the density, magnetic field, temperature, and proton fraction as locally constant. In the first place, we developed an EOS for polarized proto-neutron star matter using the nonrelativistic Hartree-Fock model with the LNS Skyrme interaction. This physical system shows an instability for low temperatures and densities which requires the Gibbs (Maxwell) construction for asymmetric (symmetric) matter. We discussed three reactions for the NMFP: the neutron and proton scattering, $\nu + n \rightarrow \nu' + n'$ and $\nu + p \rightarrow \nu' + p'$, respectively, and the absorption reaction $\nu + n \rightarrow e^- + p$. In the presence of a magnetic field, the NMFP depends on the angle between the momentum of the neutrino and the magnetic field (which we take as the \hat{z} axis). This induces an asymmetry in the mean free path which favors the flux of neutrinos parallel (antiparallel) to the magnetic field for the neutron scattering and the absorption reaction (proton scattering).

We have paid special attention to develop a self-consistent treatment of the NMFP. All the reactions also take place in free space, where the magnitude of interest is the cross section. It is not difficult to recalculate these cross sections when the reactions occur in a dense medium: the corresponding particle distribution functions are incorporated, where single-particle energies and chemical potentials are needed. There is a delicate balance between $\lambda_{\text{neut scatt}}$, $\lambda_{\text{prot scatt}}$, and λ_{neutabs} , where the effect of the medium is very important. Reliable results can only be achieved if the values for the single-particle energies and chemical potential are consistent with the density, temperature, magnetic field, and proton fraction used in the evaluation of the NMFP. It is in this sense that we understand the self-consistency of our model. In summary, our point of view is that an accurate evaluation of the NMFP requires the evaluation of the EOS on the same footing as the NMFP itself.

As mentioned, the nuclear interaction leads to an instability in the EOS for systems of two or more different kinds of particles. Within proto-neutron star matter, to restore the stability the system splits into two phases of different densities, spin and isospin composition. This two-phase system is as a whole less polarized than the unstable one-phase system. To the best of our knowledge, we have evaluated for the first time the NMFP in this two-phase region. Our results show a decrease in the NMFP asymmetry and an increase in the NMFP. Therefore, the system is more transparent and less polarized for neutrinos with respect to the unstable one-phase system.

This takes place in a density-temperature region which is not our main concern; however, its inclusion was required for completeness.

Our main concern is the asymmetry in the NMFP due to the presence of a strong magnetic field. Each channel contributing to the total NMFP exhibits a particular behavior. This is because of the Landau quantization for charged particles. Clearly this does not apply to $\lambda_{\text{neut scatt}}$, where there are no charged particles; but $\lambda_{\text{prot scatt}}$ exhibits the Landau quantization both in the initial and final states, while for λ_{neutabs} Landau levels are only in the final state. By turning off the external magnetic field, the Landau quantization disappears and $\lambda_{\text{neut scatt}}$, $\lambda_{\text{prot scatt}}$, and λ_{neutabs} have a similar functional dependence. We focus now on two aspects of this particular behavior. First, variations in the proton fraction act differently on $\lambda_{\text{neut scatt}}$ and λ_{neutabs} than on $\lambda_{\text{prot scatt}}$: as the proton fraction increases so does the partial density of protons leading to a decrease in $\lambda_{\text{prot scatt}}$, with the opposite effect on the two remaining channels. The second and more important point is that the coupling of the protons with the magnetic field is stronger than that for neutrons. This is clear from the spin asymmetry calculations. We showed that for $B = 10^{18}$ G the asymmetry in the mean free path is dominated by $\lambda_{\text{neut scatt}}$ and λ_{neutabs} . But for $B = 10^{17}$ G and symmetric matter, it is $\lambda_{\text{prot scatt}}$ which dominates this asymmetry, leading to a change of sign for this quantity. This results from the combined action of the strong and weak interactions.

Finally, we recall that we assume that temperature, baryonic density, magnetic field, and the proton fraction are locally constants. A realistic calculation of the asymmetry in the

neutrino emission from the neutron star would require a model for the distribution for these quantities as a function of the position and time, starting from its early formation, when the proton fraction is more important. As mentioned in Sec. I, one important motivation to perform these calculations is to know if the asymmetry in the neutrino emission could be the source of the so-called pulsar kick. In this work, we called attention to the dependence on the proton fraction of the asymmetry of the neutrino emission. Our results show that the presence of a strong magnetic field has a different effect on each of the three reactions that we considered. Moreover, a reliable summation of each contribution requires a self-consistent treatment with the EOS. Perhaps the evaluation of the NMFP in a system of protons, neutrons, and electrons in β equilibrium, charge neutrality, and a strong magnetic field would be the simplest realistic model to describe this problem. We understand that such a model is not available yet. From this, we believe that the asymmetry in the neutrino emission still should be considered as a possible explanation for the pulsar kick phenomenon.

ACKNOWLEDGMENTS

We thank Isaac Vidaña for his careful reading of our manuscript. E.B. is a member of the Carrera del Investigador Científico of the Consejo Nacional de Investigaciones Científicas y Técnicas (CONICET), Argentina. O.G.B. is a member of the Carrera del Investigador Científico of the Comisión de Investigaciones Científicas of the Provincia de Buenos Aires (CICPBA), Argentina.

APPENDIX A: THE STRUCTURE FUNCTION FOR THE PROTON INELASTIC SCATTERING

We recall the proton structure function defined in Eq. (51),

$$S_{s_{p_i}, s_{p_f}, N_{p_i}, N_{p_f}}^{\text{prot}} = \int_{-\infty}^{\infty} \frac{dp_{p_i, z}}{2\pi} \int_{-\infty}^{\infty} \frac{dp_{p_f, z}}{2\pi} (2\pi)^2 \delta(E_{s_{p_f}} + |p_{v_f}| - E_{s_{p_i}} - |p_{v_i}|) \times \delta(p_{p_f, z} + p_{v_f, z} - p_{p_i, z} - p_{v_i, z}) f(E_{s_{p_i}}, \mu_p, T) [1 - f(E_{s_{p_f}}, \mu_p, T)], \quad (\text{A1})$$

where $f(E_{s_p}, \mu_p, T)$ is given in Eq. (14). The single-particle energies E_{s_p} and the chemical potential μ_p are obtained from a particular model for the medium, which in our case is the Hartree-Fock approximation using the Skyrme model for the nuclear interaction. Within this model, the nucleon single-particle energy in a magnetic field is shown in Eq. (4).

Now we use the δ function representing the momentum conservation in Eq. (A1),

$$S_{s_{p_i}, s_{p_f}, N_{p_i}, N_{p_f}}^{\text{prot}} = \int_{-\infty}^{\infty} dp_{p_i, z} \delta(E_{s_{p_f}} - E_{s_{p_i}} - q_0) f(E_{s_{p_i}}, \mu_p, T) [1 - f(E_{s_{p_f}}, \mu_p, T)], \quad (\text{A2})$$

where $p_{p_f, z} = p_{p_i, z} + q_z$. We have defined $q_0 = |p_{v_i}| - |p_{v_f}|$ and the z component of the momentum transfer by the interaction can be written as $q_z = p_{v_i, z} - p_{v_f, z}$.

The remaining integral in Eq. (A2) can be done by solving the energy-conservation equation:

$$E_{s_{p_f}} - E_{s_{p_i}} - q_0 = 0. \quad (\text{A3})$$

When $m_{p, s_{p_i}}^* \neq m_{p, s_{p_f}}^*$, this equation is a polynomial of second order in $p_{p_i, z}$. After some algebra, we have

$$\alpha_p p_{p_i, z}^2 + \beta_p p_{p_i, z} + \gamma_p = 0, \quad (\text{A4})$$

where

$$\alpha_p = \frac{1}{2} \left(\frac{1}{m_{p, s_{p_f}}^*} - \frac{1}{m_{p, s_{p_i}}^*} \right), \quad \beta_p = \frac{q_z}{m_{p, s_{p_i}}^*},$$

$$\gamma_p = \frac{q_z^2}{2m_{p, s_{p_f}}^*} - q_0 + \mu_N B [2(N_{p_f} - N_{p_i}) - (s_{p_f} - s_{p_i})g_p] + \frac{1}{8}(v_{p, s_{p_f}} - v_{p, s_{p_i}}). \quad (\text{A5})$$

Note that the energy momentum of the neutrino enters into the structure function through the external quantities q_0 and q_z . Energy conservation can now be rewritten as

$$\delta(E_{s_{p_f}} - E_{s_{p_i}} - q_0) = \frac{1}{(\beta_p^2 - 4\alpha_p^2\gamma_p^2)^{1/2}} [\delta(p_{p_i,z} - p_{p_i,z}^+) + \delta(p_{p_i,z} - p_{p_i,z}^-)], \quad (\text{A6})$$

where $p_{p_i,z}^\pm$ are the roots of Eq. (A4). Finally, the expression for the structure function is given by

$$S_{s_{p_i}, s_{p_f}, N_{p_i}, N_{p_f}}^{\text{prot}} = \frac{1}{(\beta_p^2 - 4\alpha_p^2\gamma_p^2)^{1/2}} \{ f(E_{s_{p_i}}, \mu_p, T) [1 - f(E_{s_{p_f}}, \mu_p, T)] \Big|_{p_{p_i,z}=p_{p_i,z}^+} + f(E_{s_{p_i}}, \mu_p, T) [1 - f(E_{s_{p_f}}, \mu_p, T)] \Big|_{p_{p_i,z}=p_{p_i,z}^-} \}. \quad (\text{A7})$$

For the case $m_{p, s_{p_i}}^* = m_{p, s_{p_f}}^*$, we have

$$p_{p_i,z}^r = -\frac{\gamma_p}{\beta_p}, \quad (\text{A8})$$

and finally,

$$S_{s_{p_i}, s_{p_f}, N_{p_i}, N_{p_f}}^{\text{prot}} = \frac{1}{|\beta_p|} f(E_{s_{p_i}}, \mu_p, T) [1 - f(E_{s_{p_f}}, \mu_p, T)] \Big|_{p_{p_i,z}=p_{p_i,z}^r}. \quad (\text{A9})$$

APPENDIX B: PROTON SCATTERING CROSS SECTION AT $B = 0$

In this Appendix we consider the limiting case of the proton scattering cross section in Eq. (56), for $B \rightarrow 0$, showing its coincidence with the well-known expression in the absence of a magnetic field. As this task is rather involved, it is done in three steps. The first one is rather simple: we obtain the $B = 0$ limit for the weak matrix transition element. In the second step, we operate over the $B \neq 0$ cross section to obtain a certain expression. Finally, in the third step, we also operate over the $B = 0$ cross section until we arrive at the same expression as in the second step. In this way, we conclude that our $B \neq 0$ cross section has the right limit.

Step i: The weak transition matrix element from Eq. (56). From that expression, we extract the factor

$$\mathcal{W}_{\text{factor}} = \frac{1}{2} \sum_{s_{p_f}=\pm 1} [H_{\mu\alpha} L^{\mu\alpha} \Big|_{s_i=1, s_f} + H_{\mu\alpha} L^{\mu\alpha} \Big|_{s_i=-1, s_f}] S_{N_{p_i}, N_{p_f}}^{\text{prot}}, \quad (\text{B1})$$

where we have already put $A_{\text{prot}} = 0$, the value for the spin asymmetry when $B = 0$. Also, the structure function does no longer depend on the spin and it has been replaced by a common function $S_{N_{p_i}, N_{p_f}}^{\text{prot}}$. Now, from Eq. (57), it is straightforward to perform the spin summation, which leads to

$$\mathcal{W}_{\text{factor}}^{B=0} = 2 [C_V^2 (1 + \cos \theta_{v_i, v_f}) + C_A^2 (3 - \cos \theta_{v_i, v_f})] S_{N_{p_i}, N_{p_f}}^{\text{prot}}, \quad (\text{B2})$$

where we have employed

$$\cos \theta_{v_i, v_f} = \cos \theta_{v_f} \cos \theta_{v_i} + \sin \theta_{v_f} \sin \theta_{v_i} \cos \phi_{v_f}. \quad (\text{B3})$$

For the next two steps we follow the prescriptions given by Bezchastnov and Haensel [45].

Step ii: The total cross section for $B \neq 0$ in Eq. (56). For convenience, we repeat the expression for the cross section:

$$\frac{\sigma_{\text{protscatt}}(\vec{p}_{v_i})}{V} = \frac{G_F^2 eB}{2 \cdot 2\pi} \int \frac{d^3 p_{v_f}}{(2\pi)^3} \sum_{N_{p_f}=0}^{N_{p_f, \text{max}}} \sum_{s_{p_f}=\pm 1} \sum_{N_{p_i}=0}^{N_{p_i, \text{max}}} I_{N_{p_i}, N_{p_f}}^2(\omega_\perp)$$

$$\times \left[\left(\frac{1 + A_{\text{prot}}}{2} \right) S_{s_i=1, s_{p_f}, N_{p_i}, N_{p_f}}^{\text{prot}} H_{\mu\alpha} L^{\mu\alpha} \Big|_{s_i=1, s_f} + \left(\frac{1 - A_{\text{prot}}}{2} \right) S_{s_i=-1, s_{p_f}, N_{p_i}, N_{p_f}}^{\text{prot}} H_{\mu\alpha} L^{\mu\alpha} \Big|_{s_i=-1, s_f} \right].$$

Following Ref. [45], we employ

$$\sum_{N_{p_i}, N_{p_f}} \rightarrow \iint \frac{d^2 p_{\perp} d^2 p'_{\perp}}{4(eB)^2}, \quad (\text{B4})$$

$$I_{N_{p_i}, N_{p_f}}^2(\omega_{\perp}) \rightarrow \frac{2eB}{\pi \sqrt{(p_1^2 - v_{\perp}^2)(v_{\perp}^2 - p_2^2)}}, \quad (\text{B5})$$

where

$$\begin{aligned} \omega_{\perp} &= v_{\perp}^2/2eB, \\ \vec{v}_{\perp} &= (p_{v_i, x} - p_{v_f, x})\hat{i} + (p_{v_i, y} - p_{v_f, y})\hat{j}, \\ \vec{p}_{\perp} &= p_{p_i, x}\hat{i} + p_{p_i, y}\hat{j}, \\ \vec{p}'_{\perp} &= p_{p_f, x}\hat{i} + p_{p_f, y}\hat{j}, \\ \vec{p}_1 &= \vec{p}'_{\perp} + \vec{p}_{\perp}, \\ \vec{p}_2 &= \vec{p}'_{\perp} - \vec{p}_{\perp}, \\ \vec{k}_{\perp} &= p_{v_i, x}\hat{i} + p_{v_i, y}\hat{j}, \\ \vec{k}'_{\perp} &= p_{v_f, x}\hat{i} + p_{v_f, y}\hat{j}. \end{aligned}$$

Note that Eq. (B5) is discussed in Ref. [73]. For further use, we have already shown the expressions for \vec{k}_{\perp} and \vec{k}'_{\perp} .

Now we replace Eqs. (B2), (B4), and (B5), together with the definition of the structure function given in Eq. (51), into Eq. (56), and we obtain

$$\begin{aligned} \frac{\sigma_{\text{protsca}}(\vec{p}_{v_i})}{V} &= \frac{G_F^2}{(2\pi)^2} \int \dots \int \frac{d^3 p_{v_f}}{(2\pi)^3} d^2 p_{\perp} d^2 p'_{\perp} dp_{p_i, z} dp_{p_f, z} \frac{1}{\sqrt{(p_1^2 - v_{\perp}^2)(v_{\perp}^2 - p_2^2)}} \\ &\times [C_V^2(1 + \cos \theta_{v_i, v_f}) + C_A^2(3 - \cos \theta_{v_i, v_f})] \delta(E_{p_f} + |p_{v_f}| - E_{p_i} - |p_{v_i}|) \\ &\times \delta(p_{p_f, z} + p_{v_f, z} - p_{p_i, z} - p_{v_i, z}) f(E_{p_i}, \mu_p, T) [1 - f(E_{p_f}, \mu_p, T)]. \end{aligned} \quad (\text{B6})$$

Note that all eB factors have already canceled out.

Step iii: The total cross section for $B = 0$. In the absence of a magnetic field, the analytical expression for the total cross section is the same for both the neutron and proton scattering reactions. The only difference is in the values for the coupling constants C_A and C_V . We take the expression for the cross section from Ref. [53], where we have replaced the structure function for its explicit expression:

$$\begin{aligned} \frac{\sigma^{B=0}(\vec{p}_{v_i})}{V} &= \frac{G_F^2}{(2\pi)^2} \int \dots \int \frac{d^3 p_{v_f}}{(2\pi)^3} d^3 p_{p_i} d^3 p_{p_f} [C_V^2(1 + \cos \theta_{vv'}) + C_A^2(3 - \cos \theta_{vv'})] \\ &\times \delta(E_{p_f} + |p_{v_f}| - E_{p_i} - |p_{v_i}|) \delta(\vec{p}_{p_f} + \vec{p}_{v_f} - \vec{p}_{p_i} - \vec{p}_{v_i}) f(E_{p_i}, \mu_p, T) [1 - f(E_{p_f}, \mu_p, T)]. \end{aligned} \quad (\text{B7})$$

The momentum conservation can be rewritten as

$$\delta(\vec{p}_{p_f} + \vec{p}_{v_f} - \vec{p}_{p_i} - \vec{p}_{v_i}) = \delta(p_{p_f, z} + p_{v_f, z} - p_{p_i, z} - p_{v_i, z}) \delta(\vec{p}'_{\perp} + \vec{k}'_{\perp} - \vec{p}_{\perp} - \vec{k}_{\perp}). \quad (\text{B8})$$

We employ now the following identities (also from Ref. [45]):

$$d^3 p_{p_i} d^3 p_{p_f} = \frac{1}{4} dp_{p_i, z} dp_{p_f, z} d^2 p_{\perp} d^2 p'_{\perp} d\chi d\beta \quad (\text{B9})$$

and

$$R \equiv \int_0^{2\pi} d\chi \int_0^{2\pi} d\beta \delta(\vec{p}'_{\perp} + \vec{k}'_{\perp} - \vec{p}_{\perp} - \vec{k}_{\perp}) = \frac{4}{\sqrt{(p_1^2 - v_{\perp}^2)(v_{\perp}^2 - p_2^2)}}. \quad (\text{B10})$$

We refer the reader to Ref. [45] for the demonstration of the last expression. We replace these expressions in Eq. (B7), in two steps,

$$\begin{aligned} \frac{\sigma^{B=0}(\vec{p}_{v_i})}{V} &= \frac{G_F^2}{4(2\pi)^2} \int \dots \int \frac{d^3 p_{v_f}}{(2\pi)^3} d^2 p_{\perp} d^2 p'_{\perp} dp_{p_i, z} dp_{p_f, z} [C_V^2(1 + \cos \theta_{vv'}) \\ &+ C_A^2(3 - \cos \theta_{vv'})] \delta(E_{p_f} + |p_{v_f}| - E_{p_i} - |p_{v_i}|) \delta(p_{p_f, z} + p_{v_f, z} - p_{p_i, z} - p_{v_i, z}) \\ &\times R f(E_{p_i}, \mu_p, T) [1 - f(E_{p_f}, \mu_p, T)], \end{aligned} \quad (\text{B11})$$

where the replacement of R [Eq. (B10)] into this expression shows the coincidence with Eq. (B6).

Before we finish this Appendix, we should pay attention to a subtle point. Under the presence of a magnetic field, a charged particle has a value for the momentum only in the z direction, that is, p_z . In Eqs. (B4) and (B5), it is implicit that in the limit process $B \rightarrow 0$, the quantum number N is replaced by the vector $\vec{p}_\perp = p_x \hat{i} + p_y \hat{j}$. Owing to this prescription the single-particle energies in Eqs. (B6) and (B11) are the same and so is the distribution function $f(E_p, \mu_p, T)$. While the procedures in points (i) and (iii) are exact, the one in point (ii) is a reasonable assumption needed to obtain the right limit. A more complete discussion can be found in Ref. [73].

-
- [1] H. A. Bethe, *Rev. Mod. Phys.* **62**, 801 (1990).
- [2] H.-T. Janka and E. Müller, *Astron. Astrophys.* **306**, 167 (1996).
- [3] A. Burrows, *Nature (London)* **403**, 727 (2000).
- [4] H. Duan and Y.-Z. Qian, *Phys. Rev. D* **72**, 023005 (2005).
- [5] H. Duan and Y.-Z. Qian, *Phys. Rev. D* **69**, 123004 (2004).
- [6] L. F. Roberts, J. Lippuner, M. D. Duez, J. A. Faber, F. Foucart, J. C. Lombardi, Jr., S. Ning, C. D. Ott, and M. Ponce, *Mon. Not. R. Astron. Soc.* **464**, 3907 (2017).
- [7] J. J. Cowan, C. Sneden, J. E. Lawler, A. Aprahamian, M. Wiescher, K. Langanke, G. Martínez-Pinedo, and F. K. Thielemann, *Rev. Mod. Phys.* **93**, 015002 (2021).
- [8] G. Martínez-Pinedo, T. Fischer, A. Lohs, and L. Huther, *Phys. Rev. Lett.* **109**, 251104 (2012).
- [9] L. F. Roberts, S. Reddy, and G. Shen, *Phys. Rev. C* **86**, 065803 (2012).
- [10] L. F. Roberts and S. Reddy, *Phys. Rev. C* **95**, 045807 (2017).
- [11] G. Guo, G. Martínez-Pinedo, A. Lohs, and T. Fischer, *Phys. Rev. D* **102**, 023037 (2020).
- [12] A. Burrows and J. M. Lattimer, *Astrophys. J.* **307**, 178 (1986).
- [13] W. Keil and H.-T. Janka, *Astron. Astrophys.* **296**, 145 (1995).
- [14] J. A. Pons, S. Reddy, M. Prakash, J. M. Lattimer, and J. A. Miralles, *Astrophys. J.* **513**, 780 (1999).
- [15] Y. A. Shibhanov and D. G. Yakovlev, *Astron. Astrophys.* **309**, 171 (1996).
- [16] D. G. Yakovlev and C. J. Pethick, *Annu. Rev. Astron. Astrophys.* **42**, 169 (2004).
- [17] A. Perego, S. Rosswog, R. Cabezón, O. Korobkin, R. Kaeppli, A. Arcones, and M. Liebendoerfer, *Mon. Not. R. Astron. Soc.* **443**, 3134 (2014).
- [18] D. Martin, A. Perego, A. Arcones, F.-K. Thielemann, O. Korobkin, and S. Rosswog, *Astrophys. J.* **813**, 2 (2015).
- [19] M. Frensel, M.-R. Wu, C. Volpe, and A. Perego, *Phys. Rev. D* **95**, 023011 (2017).
- [20] M. Cusinato, F. M. Guercilena, A. Perego, D. Logoteta, D. Radice, S. Bernuzzi, and S. Ansoldi, *Eur. Phys. J. A* **58**, 99 (2022).
- [21] D. Radice, S. Bernuzzi, A. Perego, and R. Haas, *Mon. Not. R. Astron. Soc.* **512**, 1499 (2022).
- [22] D. G. Yakovlev, A. D. Kaminker, O. Y. Gnedin, and P. Haensel, *Phys. Rep.* **354**, 1 (2001).
- [23] G. Guo and Y.-Z. Qian, *Phys. Rev. D* **94**, 043005 (2016).
- [24] R. C. Duncan and C. Thompson, *Astrophys. J.* **392**, L9 (1992).
- [25] J. Cordes, R. Romani, and S. Lundgren, *Nature (London)* **362**, 133 (1993).
- [26] A. Kusenko and G. Segrè, *Phys. Rev. Lett.* **77**, 4872 (1996).
- [27] C. J. Horowitz and G. Li, *Phys. Rev. Lett.* **80**, 3694 (1998).
- [28] V. L. Kauts, A. M. Savochkin, and A. I. Studenikin, *Phys. At. Nucl.* **69**, 1453 (2006).
- [29] T. Maruyama, N. Yasutake, M.-K. Cheoun, J. Hidaka, T. Kajino, G. J. Mathews, and C.-Y. Ryu, *Phys. Rev. D* **86**, 123003 (2012).
- [30] T. Maruyama, M. K. Cheoun, J. Hidaka, T. Kajino, T. Kuroda, G. J. Mathews, C. Y. Ryu, T. Takiwaki, and N. Yasutake, *Phys. Rev. D* **90**, 067302 (2014).
- [31] D. Tubbs and D. Schramm, *Astrophys. J.* **201**, 467 (1975).
- [32] R. F. Sawyer, *Phys. Rev. D* **11**, 2740 (1975).
- [33] N. Iwamoto and C. J. Pethick, *Phys. Rev. D* **25**, 313 (1982).
- [34] S. O. Bäckman, C. G. Källman, and O. Sjöberg, *Phys. Lett. B* **43**, 263 (1973).
- [35] P. Haensel and A. J. Jerzak, *Astron. Astrophys.* **179**, 127 (1987).
- [36] C. J. Horowitz and K. Wehrberger, *Nucl. Phys. A* **531**, 665 (1991).
- [37] S. Reddy and M. Prakash, *Astrophys. J.* **478**, 689 (1997).
- [38] S. Reddy, M. Prakash, and J. M. Lattimer, *Phys. Rev. D* **58**, 013009 (1998).
- [39] S. Reddy, M. Prakash, J. M. Lattimer, and J. A. Pons, *Phys. Rev. C* **59**, 2888 (1999).
- [40] S. Reddy, Ph.D. thesis, State University of New York at Stony Brook, 1998.
- [41] A. Burrows and R. F. Sawyer, *Phys. Rev. C* **58**, 554 (1998).
- [42] J. Navarro, E. S. Hernández, and D. Vautherin, *Phys. Rev. C* **60**, 045801 (1999).
- [43] C. Shen, U. Lombardo, N. Van Giai, and W. Zuo, *Phys. Rev. C* **68**, 055802 (2003).
- [44] J. Margueron, I. Vidaña, and I. Bombaci, *Phys. Rev. C* **68**, 055806 (2003).
- [45] V. G. Bezchastnov and P. Haensel, *Phys. Rev. D* **54**, 3706 (1996).
- [46] P. Arras and D. Lai, *Phys. Rev. D* **60**, 043001 (1999).
- [47] D. Chandra, A. Goyal, and K. Goswami, *Phys. Rev. D* **65**, 053003 (2002).
- [48] S. Ando, *Phys. Rev. D* **68**, 063002 (2003).
- [49] C. J. Horowitz and A. Schwenk, *Phys. Lett. B* **642**, 326 (2006).
- [50] I. Sagert and J. Schaffner-Bielich, *Astron. Astrophys.* **489**, 281 (2008).
- [51] M. A. Pérez-García, *Phys. Rev. C* **80**, 045804 (2009).
- [52] M. Ángeles Pérez-García, *Eur. Phys. J. A* **44**, 77 (2010).
- [53] J. Torres Patiño, E. Bauer, and I. Vidaña, *Phys. Rev. C* **99**, 045808 (2019).
- [54] E. Bauer and J. Torres Patiño, *Phys. Rev. C* **101**, 065806 (2020).
- [55] L. G. Cao, U. Lombardo, C. W. Shen, and N. V. Giai, *Phys. Rev. C* **73**, 014313 (2006).
- [56] R. Aguirre and E. Bauer, *J. Phys. G: Nucl. Part. Phys.* **42**, 105101 (2015).
- [57] N. K. Glendenning, *Phys. Rev. D* **46**, 1274 (1992).
- [58] H. Müller and B. D. Serot, *Phys. Rev. C* **52**, 2072 (1995).
- [59] Ph. Chomaz, M. Colonna, and J. Randrup, *Phys. Rep.* **389**, 263 (2004).
- [60] C. Ducoin, Ph. Chomaz, and F. Gulminelli, *Nucl. Phys. A* **771**, 68 (2006).

- [61] D. G. Ravenhall, C. J. Pethick, and J. R. Wilson, *Phys. Rev. Lett.* **50**, 2066 (1983).
- [62] X. Wang, J. Li, J. Fang, H. Pais, and C. Providência, *Phys. Rev. D* **105**, 063004 (2022).
- [63] M. Ferreira, A. Rabhi, and C. Providência, *Eur. Phys. J. A* **57**, 263 (2021).
- [64] C. Cohen-Tannoudji, B. Diu, and F. Laloë, *Quantum Mechanics* (Hermann and John Wiley & Sons, New York, 1977).
- [65] W. Greiner and J. Reinhard, *Field Quantization* (Springer-Verlag, Berlin, 1996).
- [66] J. D. Bjorken and S. D. Drell, *Relativistic Quantum Mechanics* (McGraw-Hill, New York, 1964).
- [67] *Handbook of Mathematical Functions*, edited by M. Abramowitz and I. A. Stegun (Dover, New York, 1972).
- [68] A. A. Sokolov and I. M. Ternov, *Synchrotron Radiation* (Pergamon Press, Oxford, 1968).
- [69] R. B. Wiringa, V. G. J. Stoks, and R. Schiavilla, *Phys. Rev. C* **51**, 38 (1995).
- [70] B. S. Pudliner, V. R. Pandharipande, J. Carlson, and R. B. Wiringa, *Phys. Rev. Lett.* **74**, 4396 (1995).
- [71] For a discussion of this factor see Appendix A in Ref. [54].
- [72] O. G. Benvenuto, E. Bauer, and I. Vidaña, [arXiv:2304.08776](https://arxiv.org/abs/2304.08776).
- [73] A. D. Kaminker and D. G. Yakovlev, *Theor. Math. Phys.* **49**, 1012 (1981).